

Figure 1. Basaltic volcanic rocks of the Western Great Basin since about 12 Ma. Data from Luedke and Smith (1981) and references in Connor and Hill (1994) and U.S. Nuclear Regulatory Commission (1999). Dashed area represents zone used to calculate background Quaternary volcano recurrence rates, which does not encompass the Long Valley Caldera magmatic system. Coordinates in Universal Transverse Mercator meters, Zone 11, NAD27.

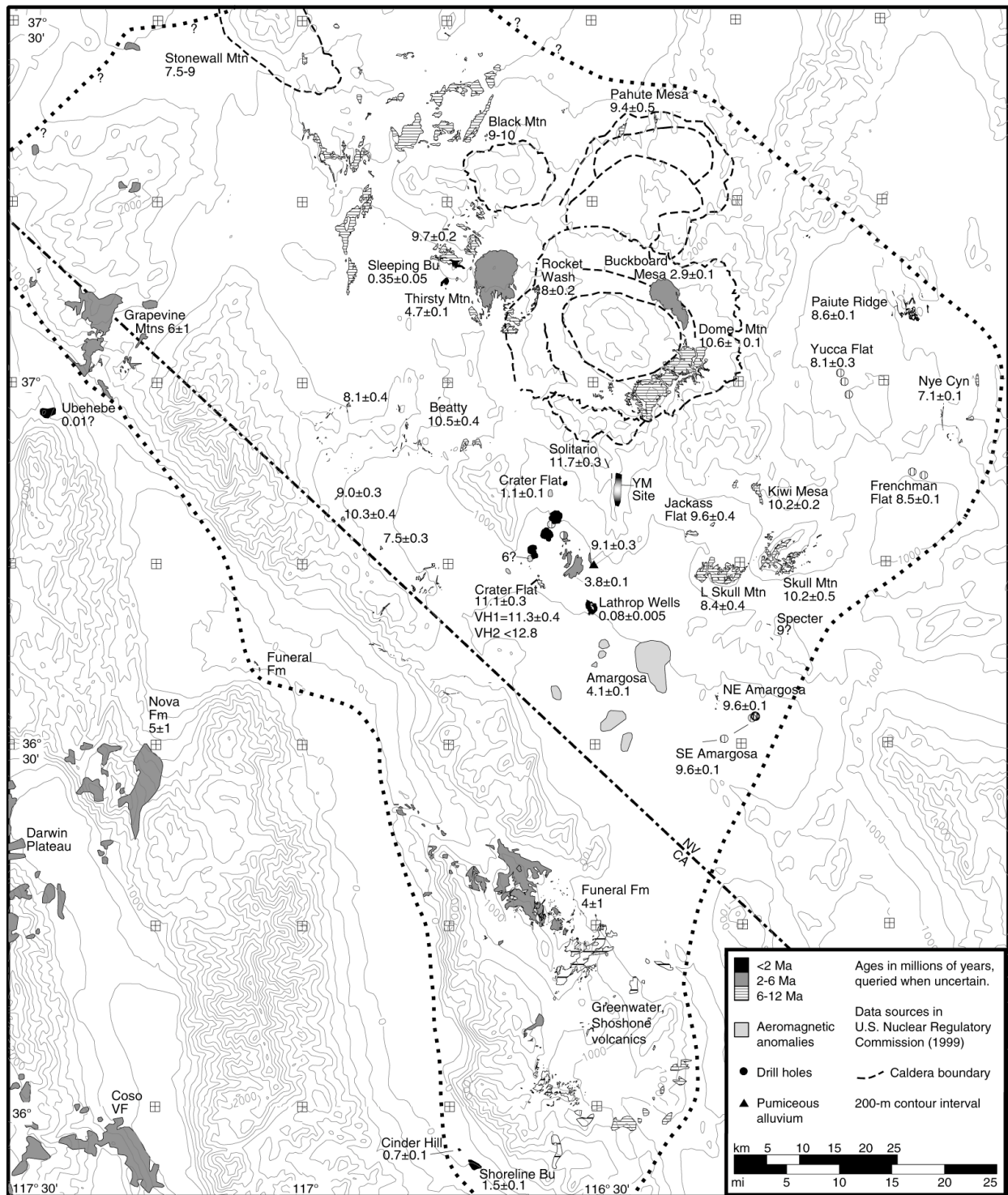


Figure 2. Basaltic volcanic rocks of the Yucca Mountain region since about 11 Ma. Data sources listed in U.S. Nuclear Regulatory Commission (1999). Dotted line represents the extent of basaltic volcanic rocks that potentially constitute the Yucca Mountain region magma system.

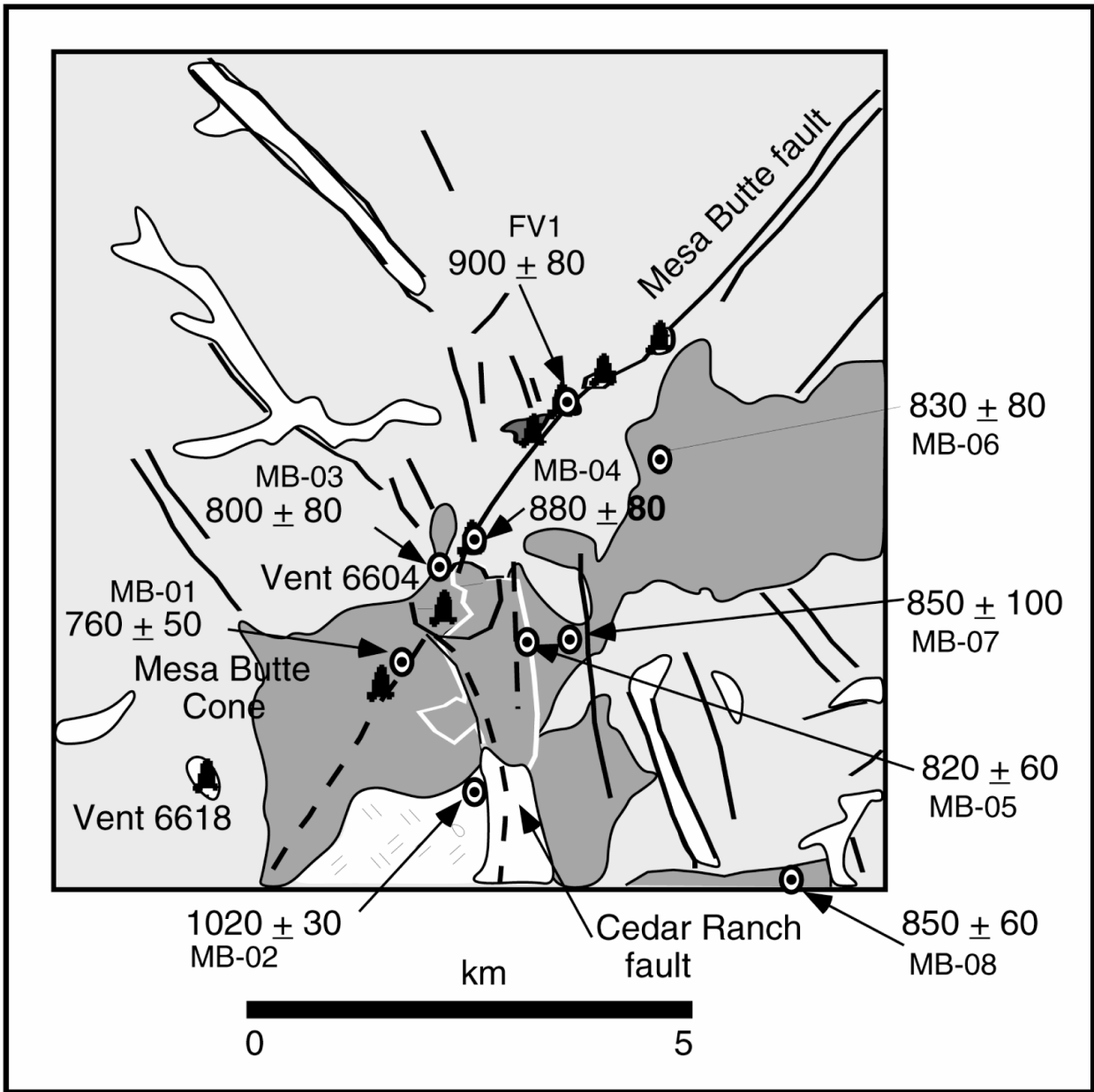


Figure 3. Development of multiple vent alignments along a fault is illustrated by the Mesa Butte alignment in the San Francisco volcanic field, Arizona. Dated cones and associated lava flows show that this 20-km-long alignment developed by repeated injection of magma along the Mesa Butte fault. Figure from Conway, et al. (1997).

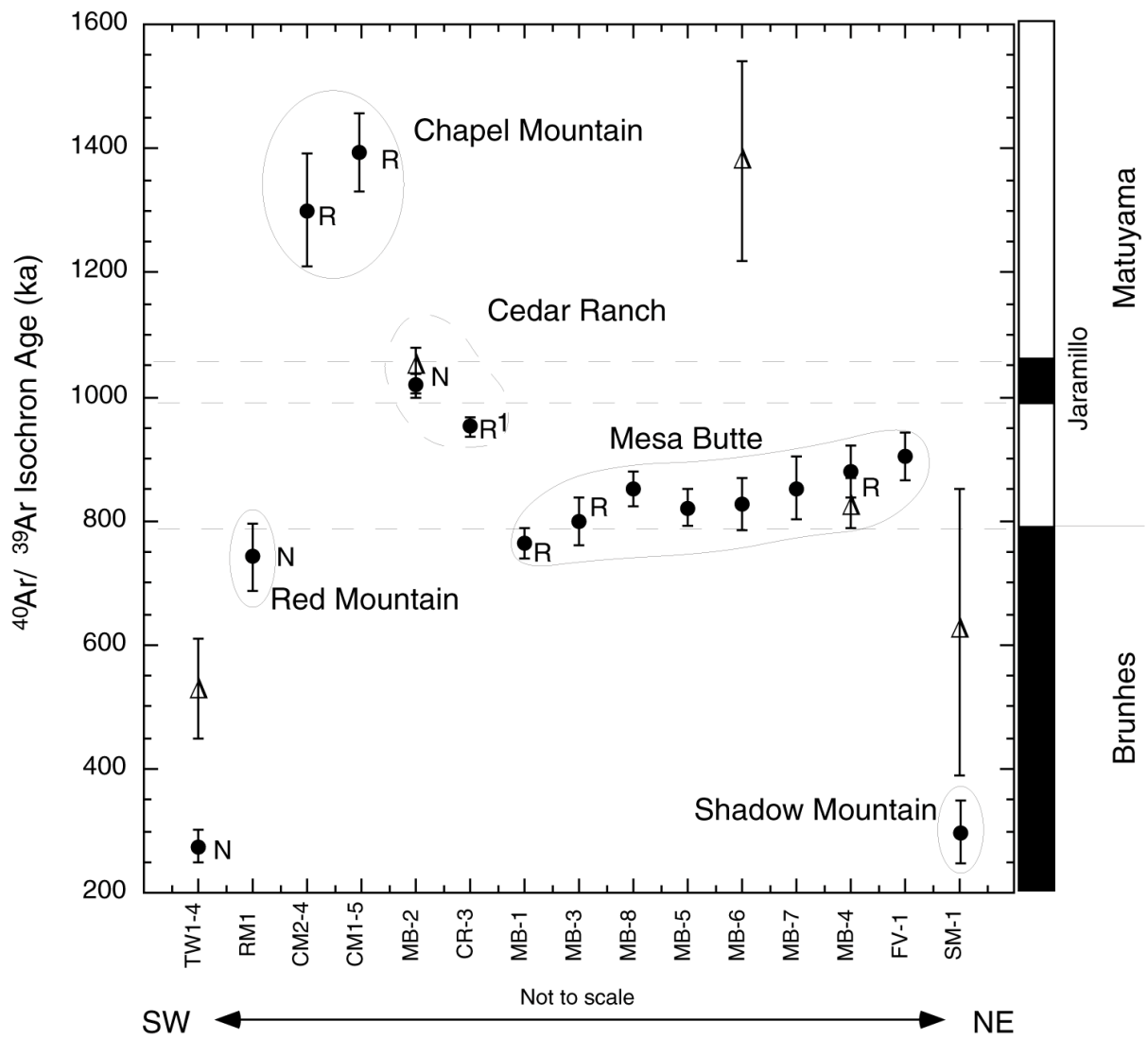


Figure 4. Detailed geochronology shows that the Mesa Butte alignment formed during a period of more than 1 m.y. through several distinct episodes of volcanism. Figure from Conway, et al. (1997).

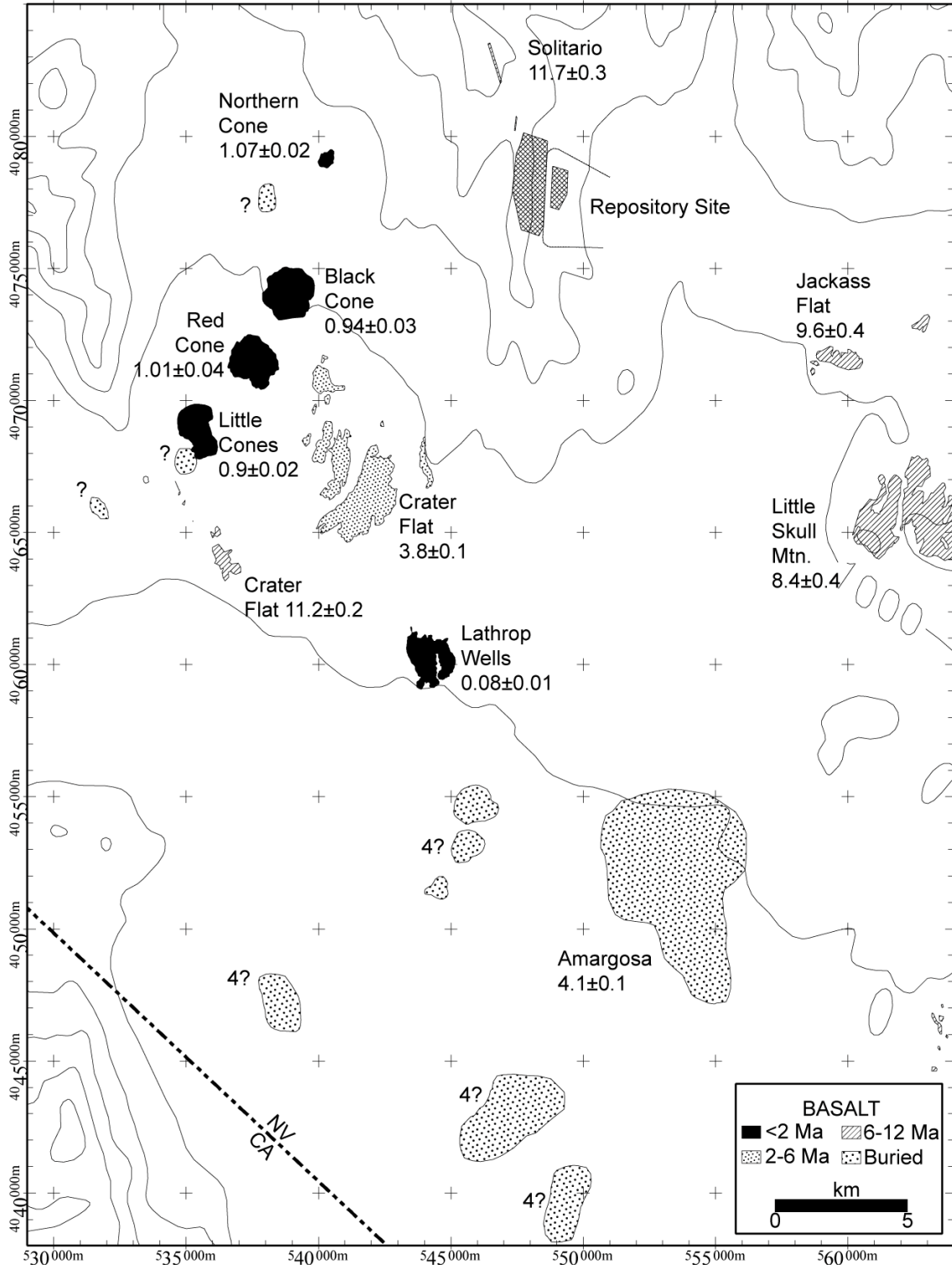


Figure 5. Basaltic volcanic rocks of the Crater Flat area, Nevada. Data sources listed in U.S. Nuclear Regulatory Commission (1999), ages queried when uncertain or unknown. Extent of buried anomalies interpreted from magnetic data in Langenheim, et al. (1993), Connor, et al. (1997), and Magsino, et al. (1998).

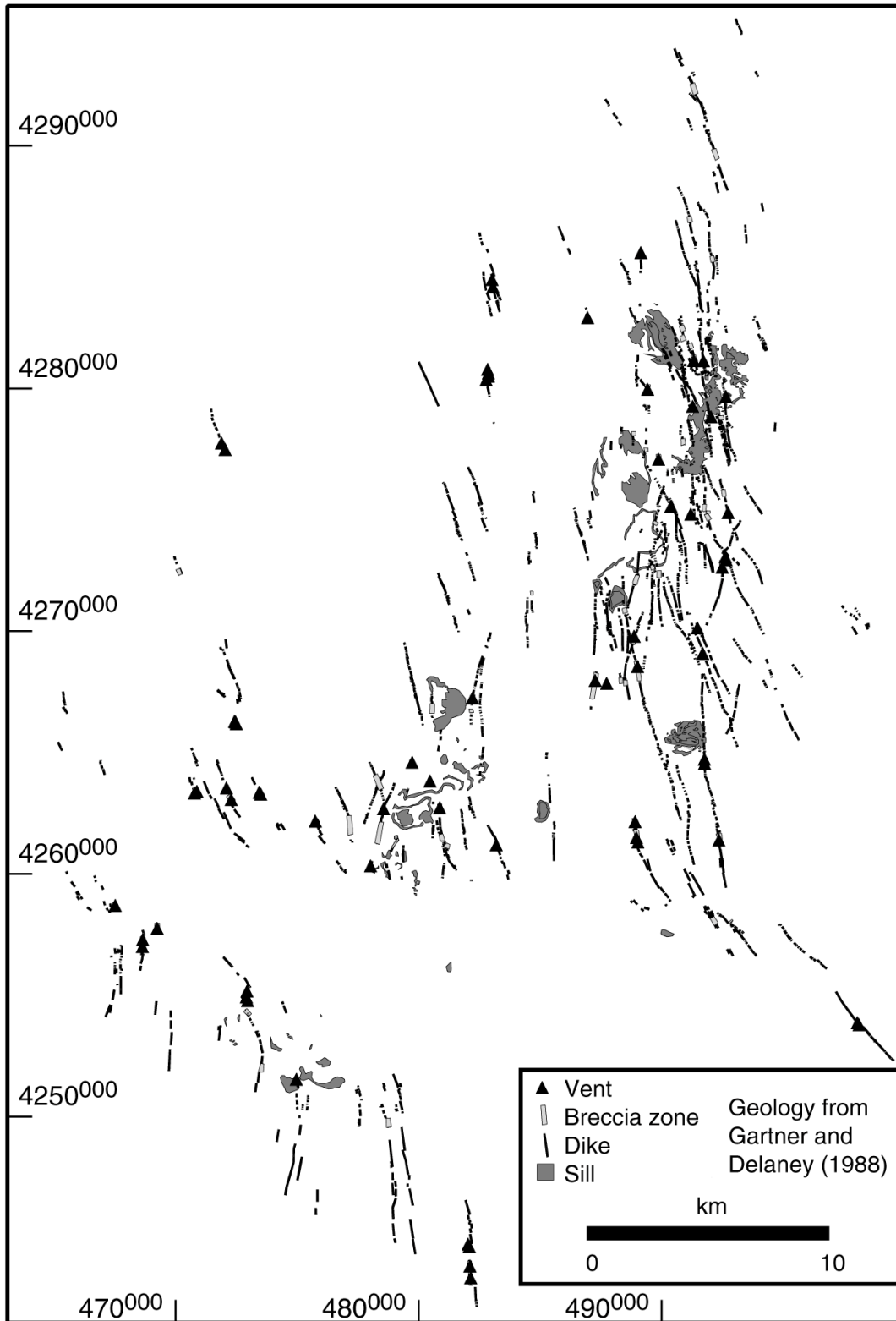


Figure 6. Distribution of dikes, breccia zones, sills, and vents in the San Rafael volcanic field, Utah. Figure from map by Gartner and Delaney (1988).

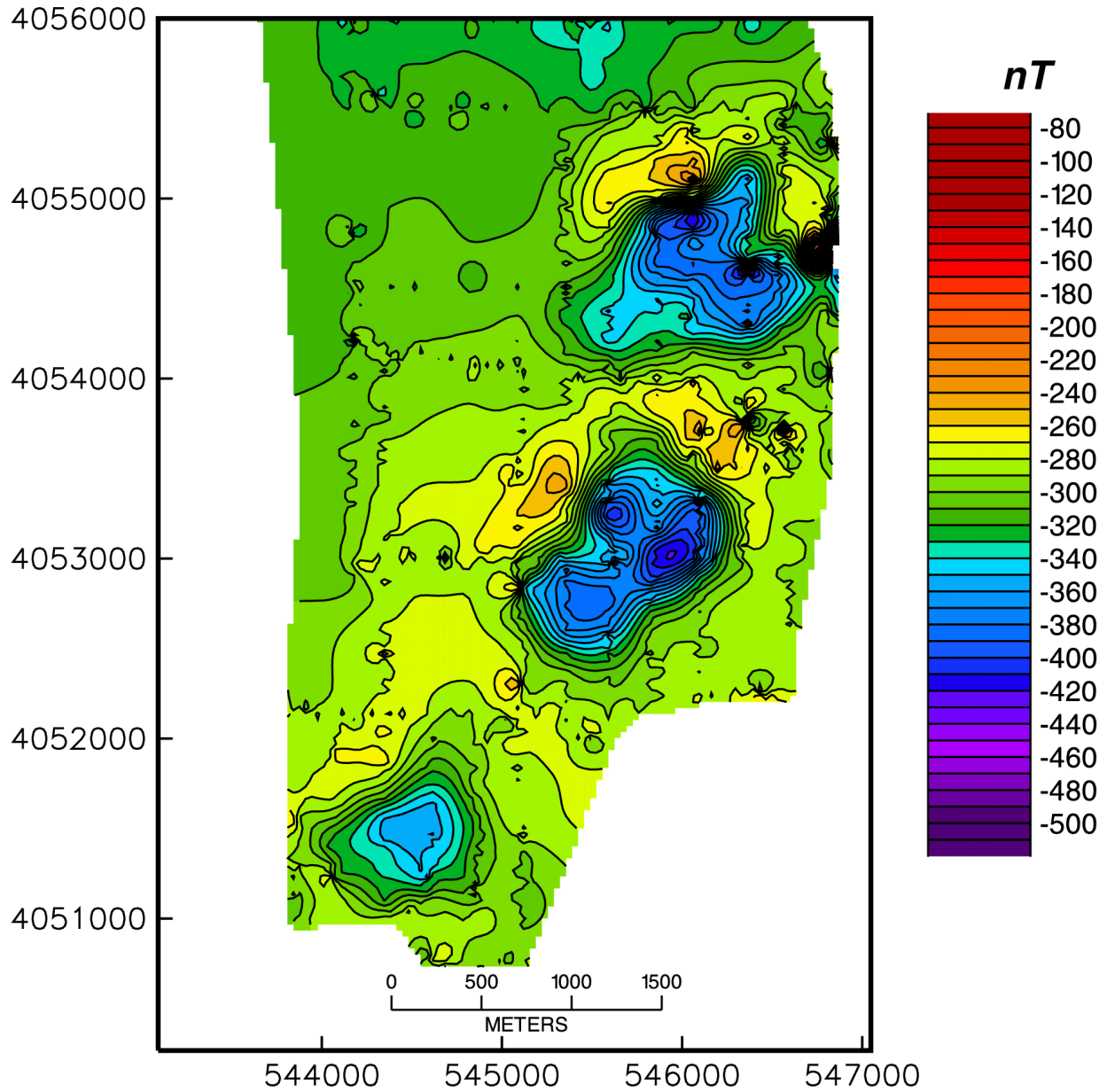


Figure 7. Ground magnetic map of Amargosa Aeromagnetic Anomaly A showing three aligned anomalies, interpreted to be produced by a buried alignment of three basaltic volcanoes. Contour interval is 10 nT. Figure from Connor, et al. (1997).

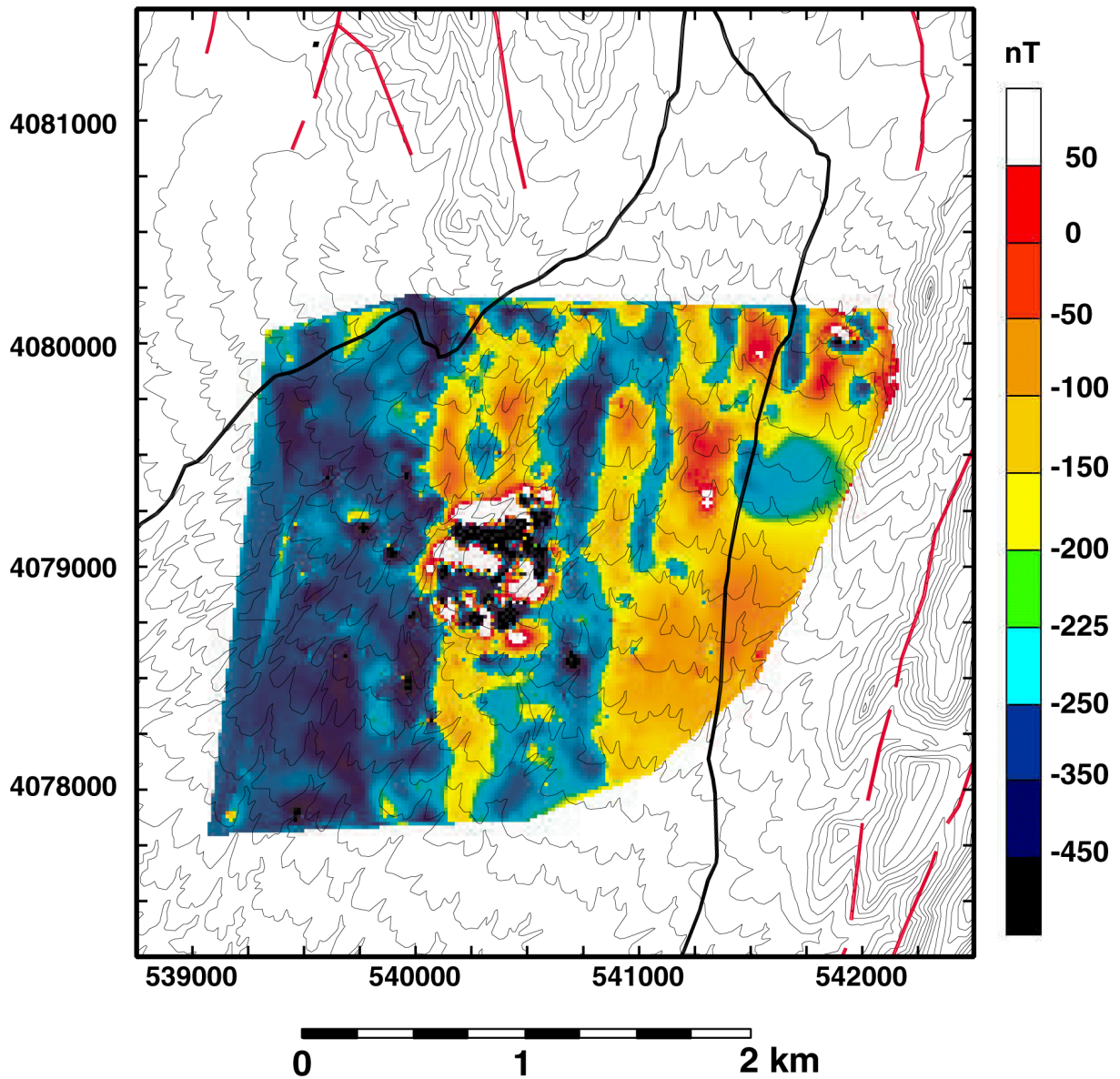


Figure 8. Ground magnetic map of the Northern Cone area, Crater Flat, Nevada. Northern Cone is located in the central part of the map, as indicated by high-amplitude, short-wavelength anomalies. North-trending anomalies are interpreted to be produced by faults that displace tuff beneath the thin alluvial cover. Figure from Connor, et al. (1997).

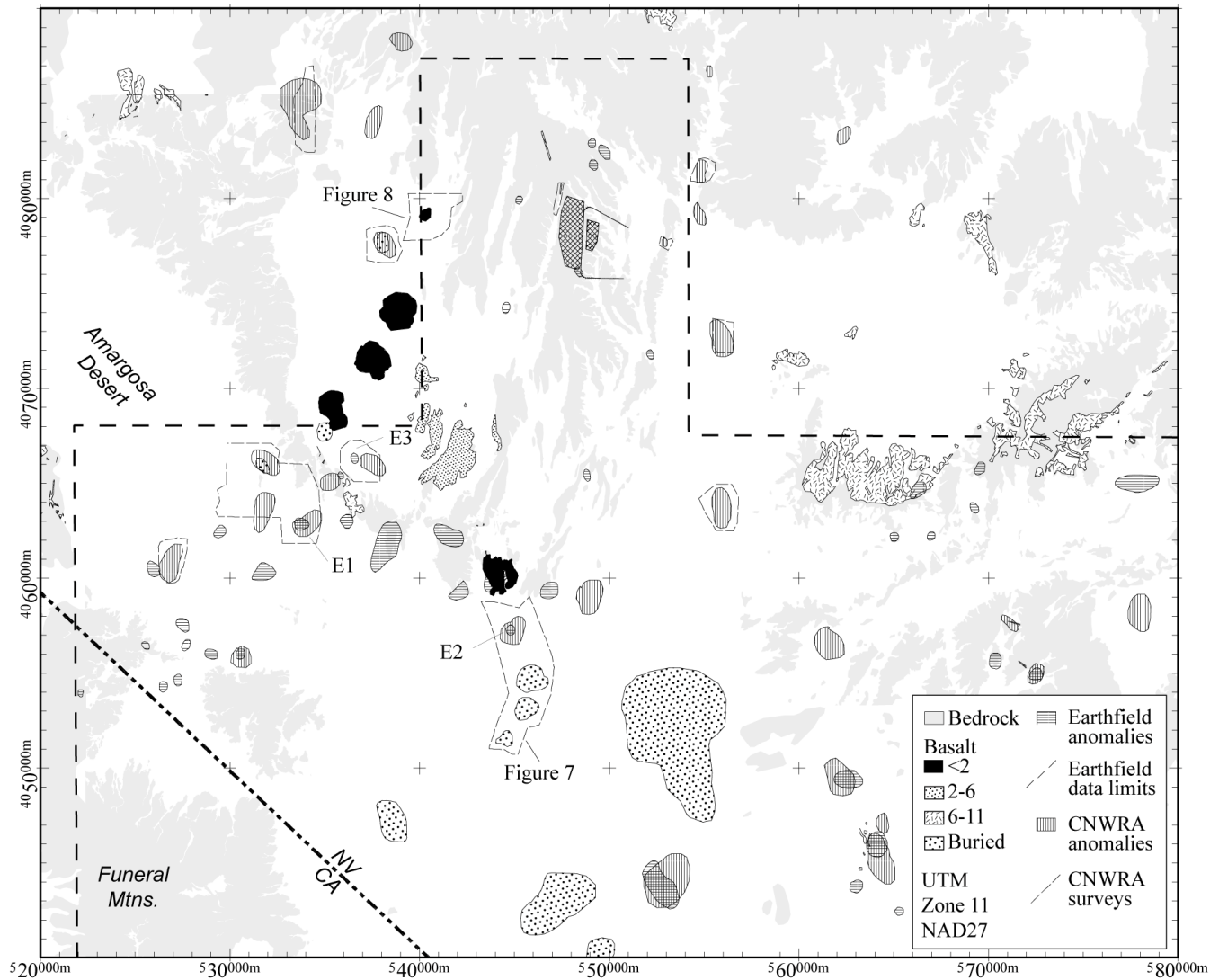


Figure 9. Location of interpreted igneous intrusions from Earthfield (1995) (horizontal lines). Aeromagnetic anomalies interpreted by CNWRA staff as possibly related to buried basaltic rocks (vertical lines), extent of CNWRA ground-magnetic surveys (Magsino, et al., 1998), and basaltic volcanic rocks of the YMR. Anomalies labeled “E1” and “E2” correspond to Earthfield (1995) anomalies likely related to small, buried basaltic features. Anomaly “E3” relates to faulted tuffaceous bedrock.

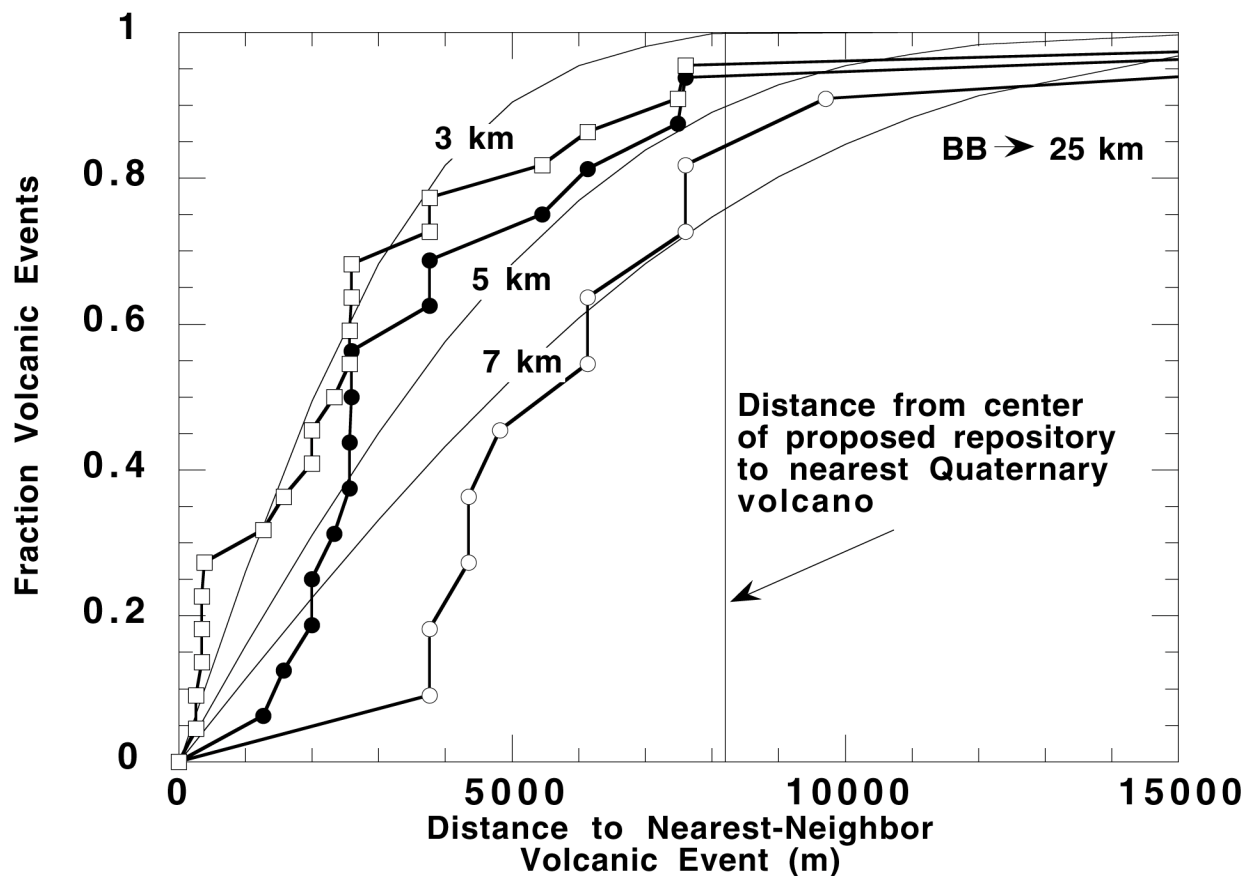


Figure 10. Comparison of observed fraction of volcanoes within a given distance of their nearest-neighbor volcano with Gaussian kernel models calculated using $h = 3$ km, 5 km, and 7 km. Observed curves include all vents (open squares), all vents or vent pairs more closely spaced than 1 km (solid circles), and vents and vent alignments (open circles). Buckboard Mesa (BB) is an outlier in the distribution as it is approximately 25 km from its nearest neighbor. The center of the repository site is located 8.2 km from Northern Cone, the nearest Quaternary volcano.

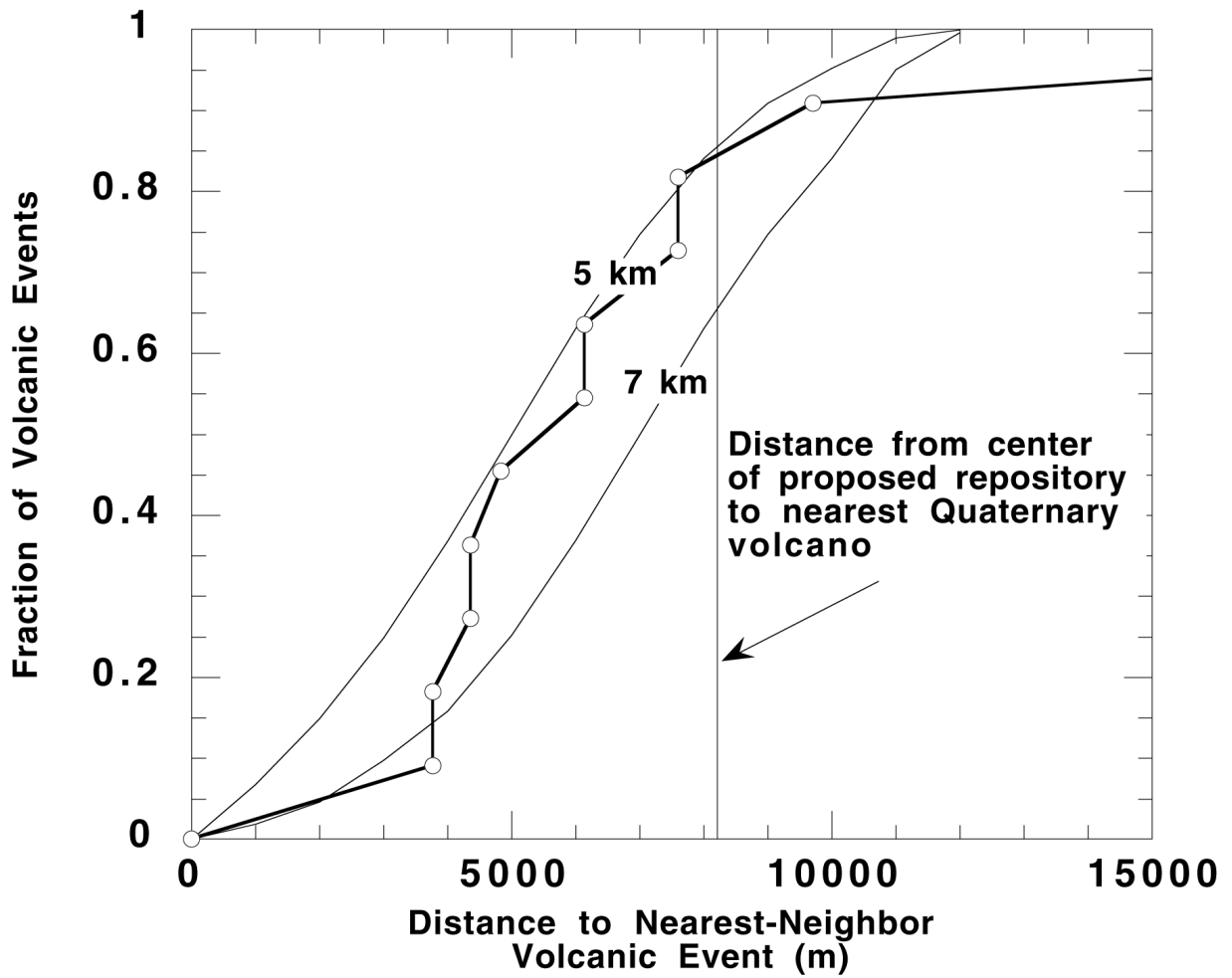


Figure 11. Comparison of observed fraction of volcanic events within a given distance of their nearest-neighbor volcano with Gaussian kernel models calculated using $h = 5$ km and 7 km. Observed curves include vents and vent alignments (open circles) as single volcanic events calculated from the center of the vent alignment. Buckboard Mesa is an outlier in the distribution as it is approximately 25 km from its nearest neighbor.

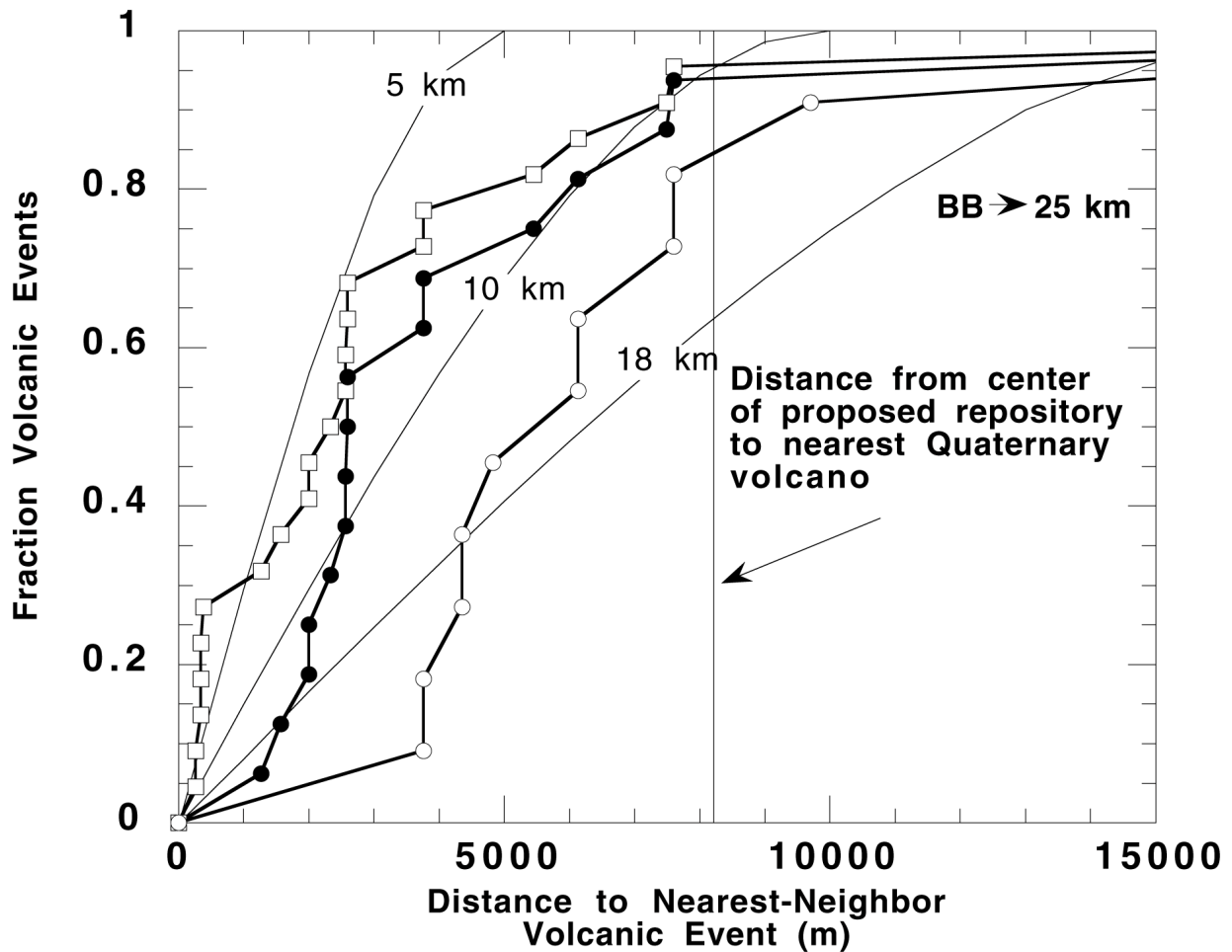


Figure 12. Comparison of observed fraction of volcanoes within a given distance of their nearest-neighbor volcano with Epanechnikov kernel models calculated using $h = 5$ km, 10 km, and 18 km. Observed curves include all vents (open squares), all vents or vent pairs more closely spaced than 1 km (solid circles), and vents and vent alignments (open circles). Buckboard Mesa (BB) is an outlier in the distribution as it is approximately 25 km from its nearest neighbor. The center of the repository site is located 8.2 km from Northern Cone, the nearest Quaternary volcano.

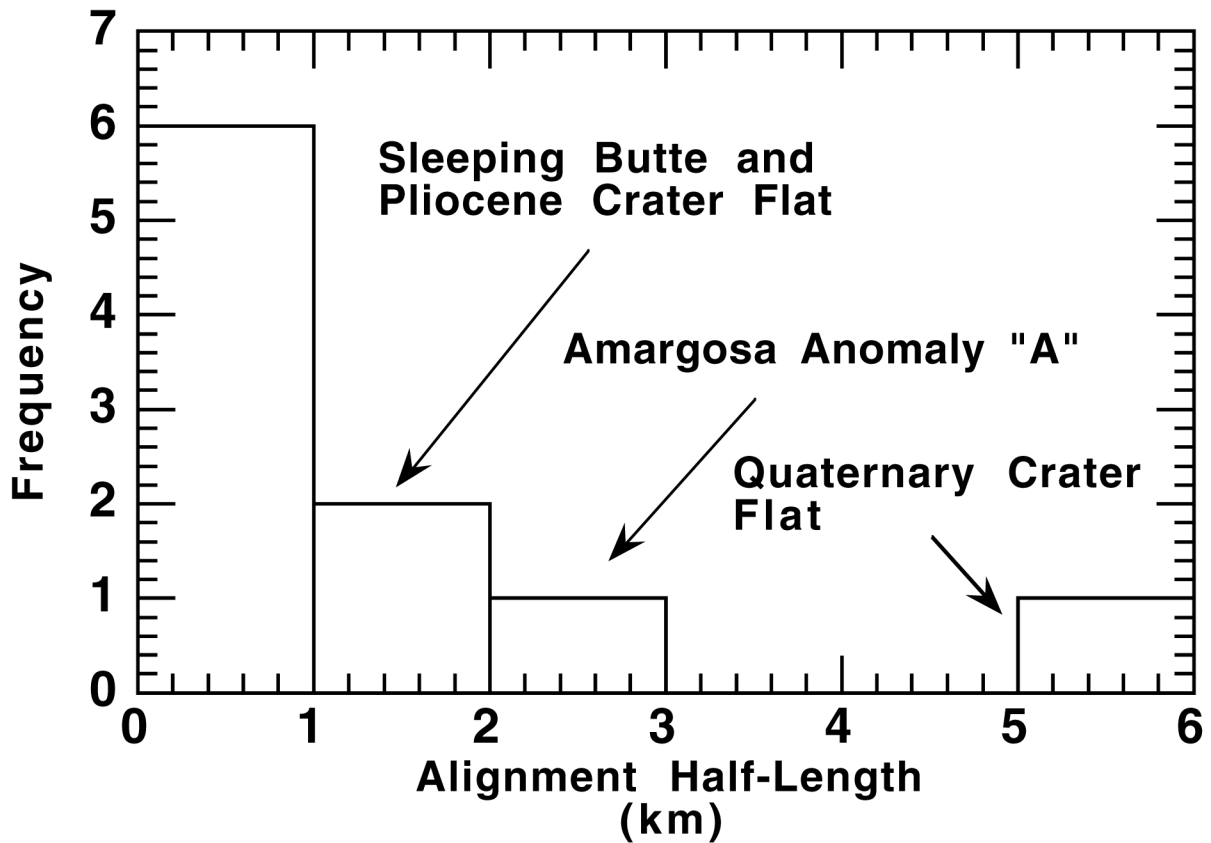


Figure 13. Distribution of Plio-Quaternary vents by vent alignment half-length. Most vents in the Yucca Mountain region occur as isolated vents. The youngest and longest vent alignment in the Yucca Mountain region, the Quaternary Crater Flat Alignment, is also closest to the repository site.

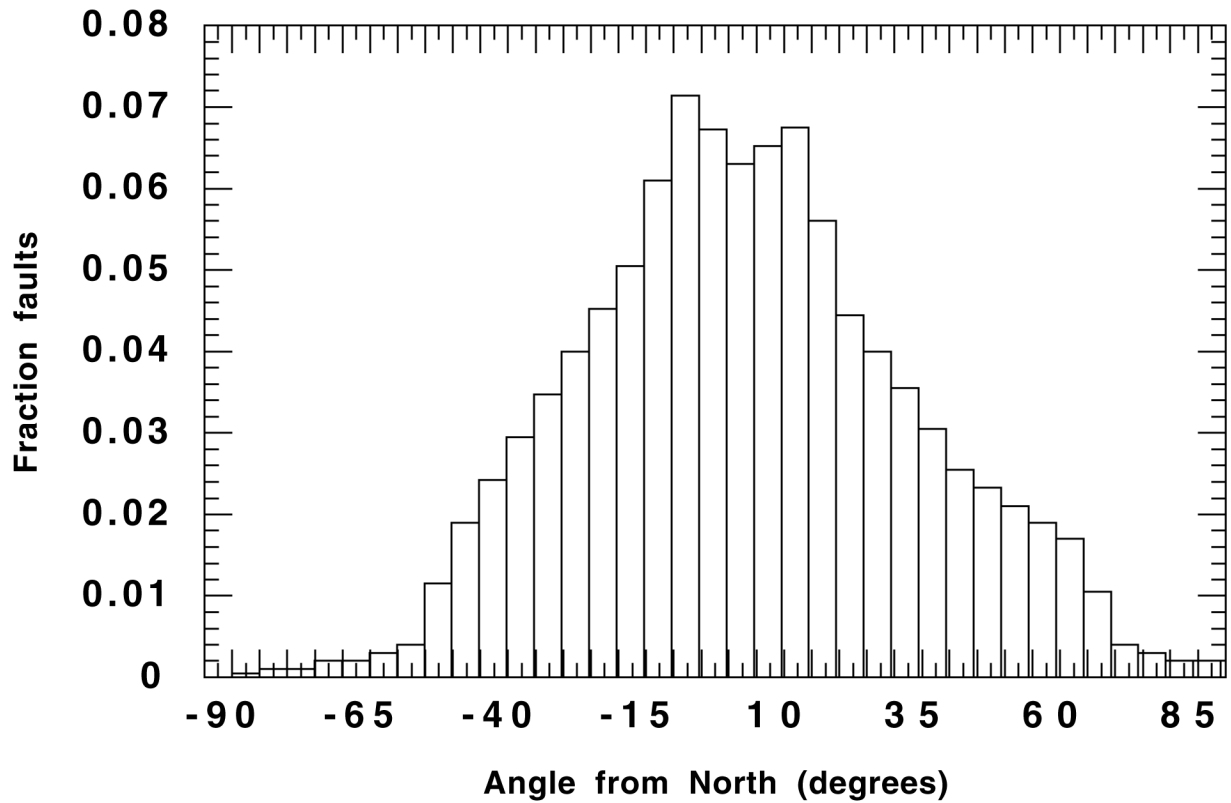


Figure 14. Distribution of the orientation of fault segments with respect to north. This distribution is weighted by fault segment length. Near the repository, $f_{\phi}(\varphi)$ may vary as a function of this distribution of fault orientations if ascending magmas follow fault planes to the surface.

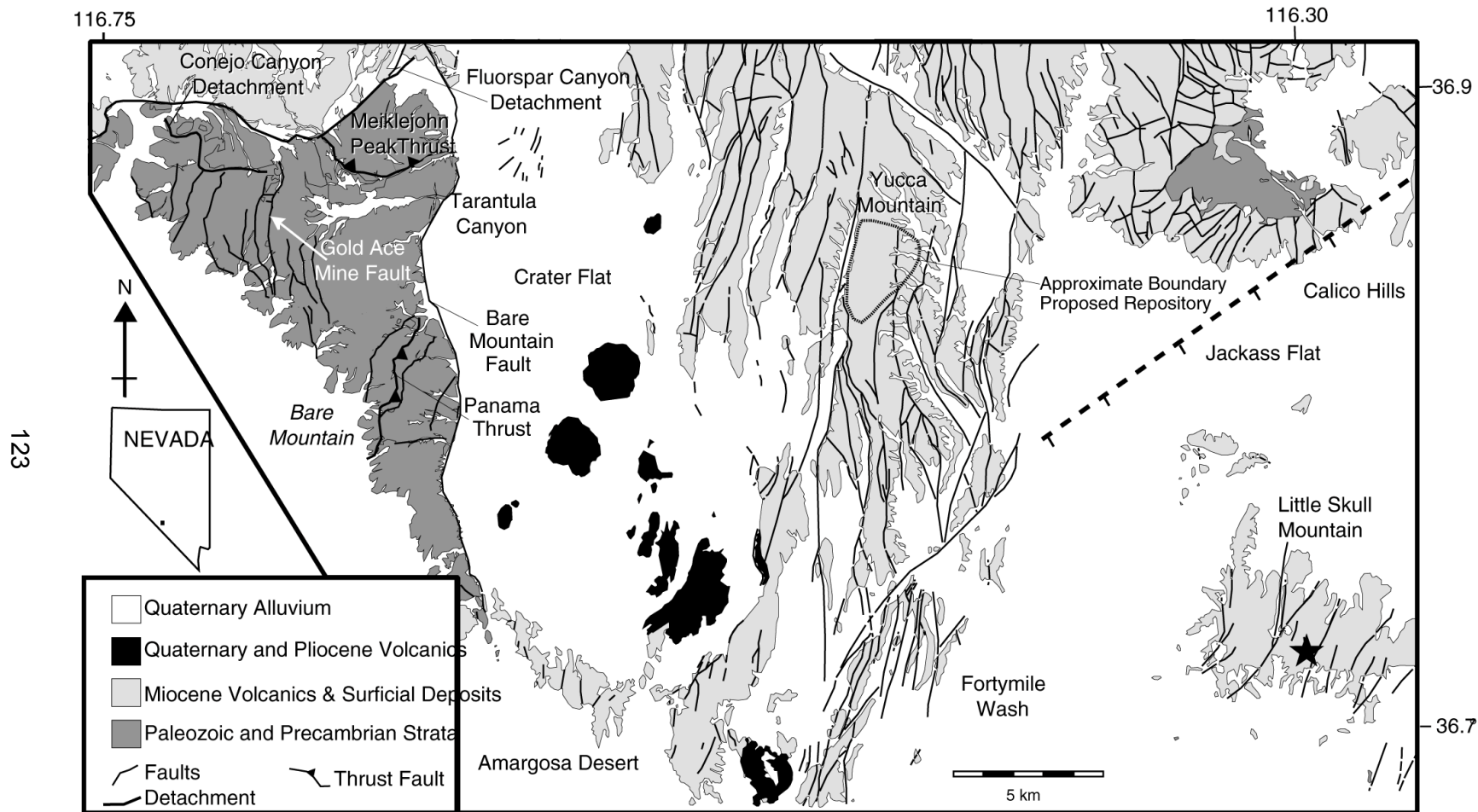


Figure 15. Simplified geologic map of the area around Yucca Mountain showing major geologic units, including Plio-Quaternary volcanoes and faults. From Ferrill, et al. (1996).

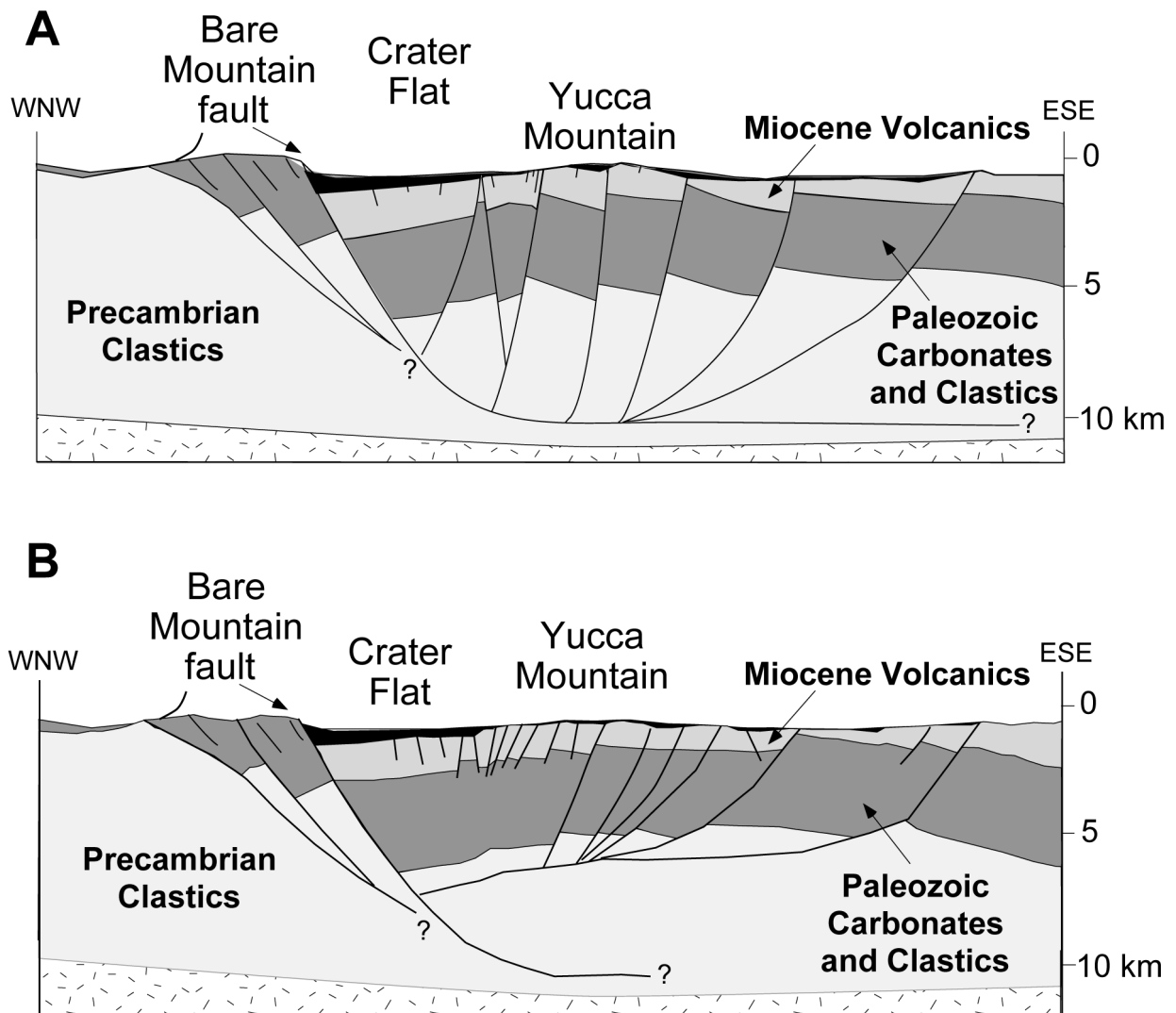


Figure 16. Two balanced cross sections across Bare Mountain, Crater Flat, and Yucca Mountain (from Ferrill, et al., 1996). The cross sections differ in the depth of the detachment fault. High-angle normal faults at Yucca Mountain intersect this detachment at depths between 5 km (b) and 10 km (a). The high dilation-tendency faults may serve as pathways for ascending magmas.

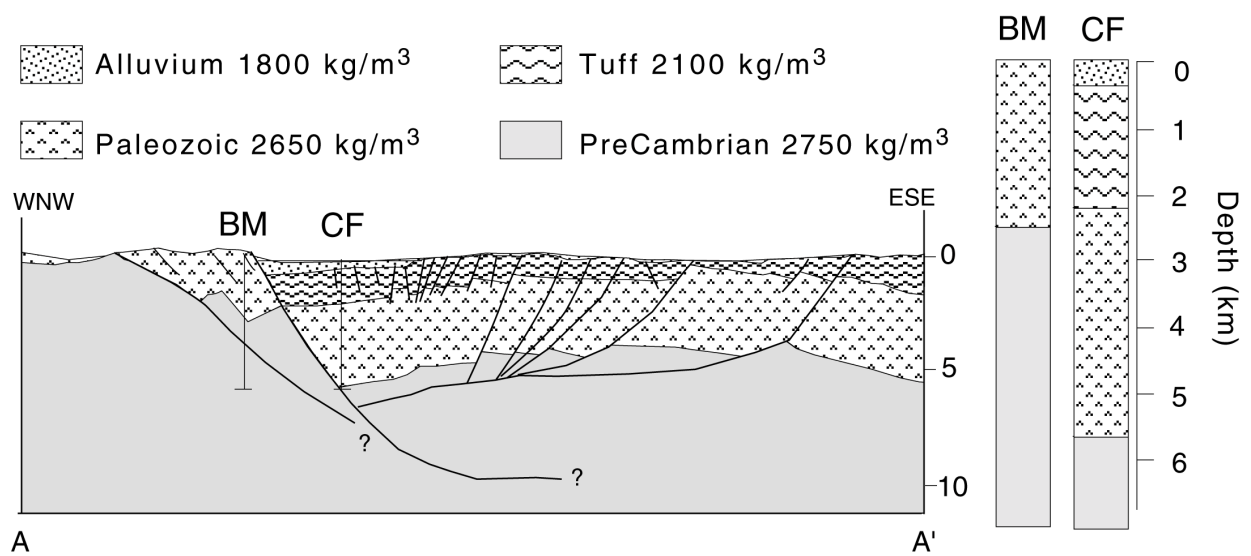


Figure 17. Comparison of density profiles beneath Bare Mountain (BM) and Crater Flat (CF). Profiles are constructed using a balanced cross-section (Ferrill et al., 1996) and density values from McKague (1980) and Howard (1985). Density differences are assumed to be negligible beneath 5.6 km.

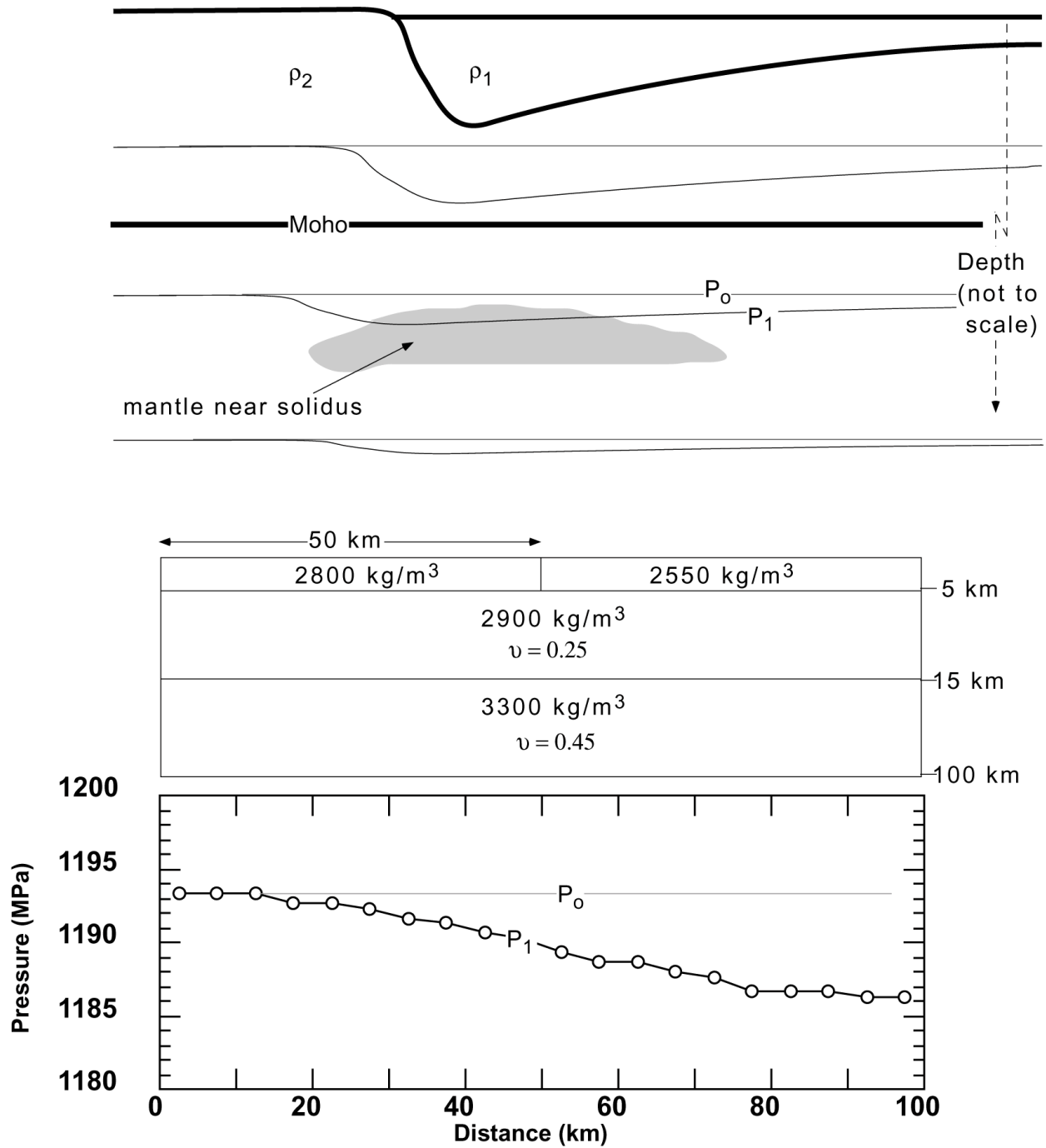


Figure 18. Conceptual model of melt generation in response to crustal extension. (a) [upper Figure] Extension results in lateral density contrast in the crust that deflects isopressure surfaces downward to P_1 from their initial depth P_0 . This local decrease in pressure results in the partial melting of near-solidus mantle. A simple finite element model (b) [lower Figure] indicates that pressure changes of 7 MPa are expected at depths of 40 km in response to large density variations in the upper 5 km of the crust, using the bulk densities and values of Poisson's ratio, ν , indicated in text.

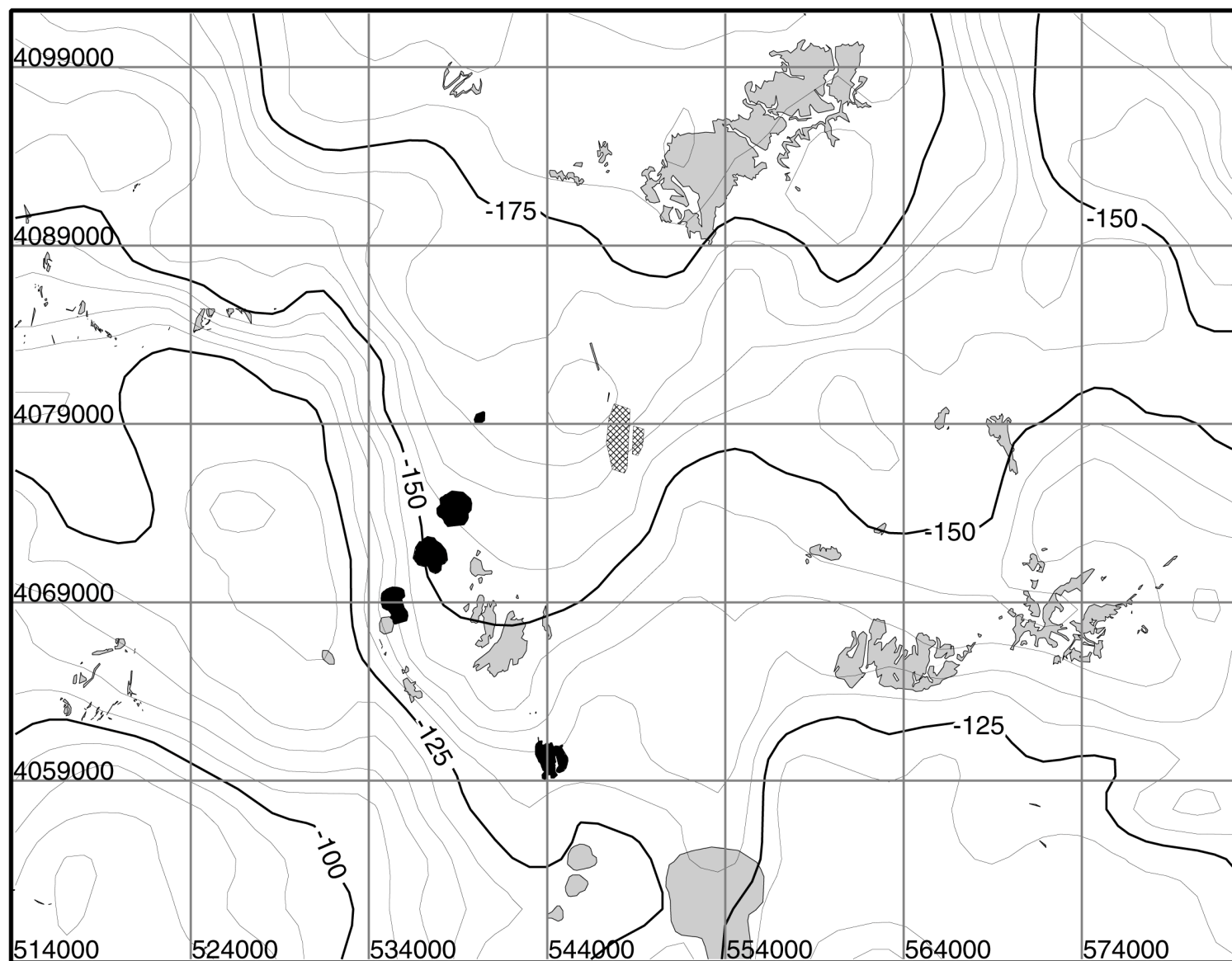


Figure 19. Bouguer gravity anomaly map of the Yucca Mountain region. Data compiled from numerous sources and obtained from Geophysics Data Repository at Lawrence Berkeley National Laboratory.

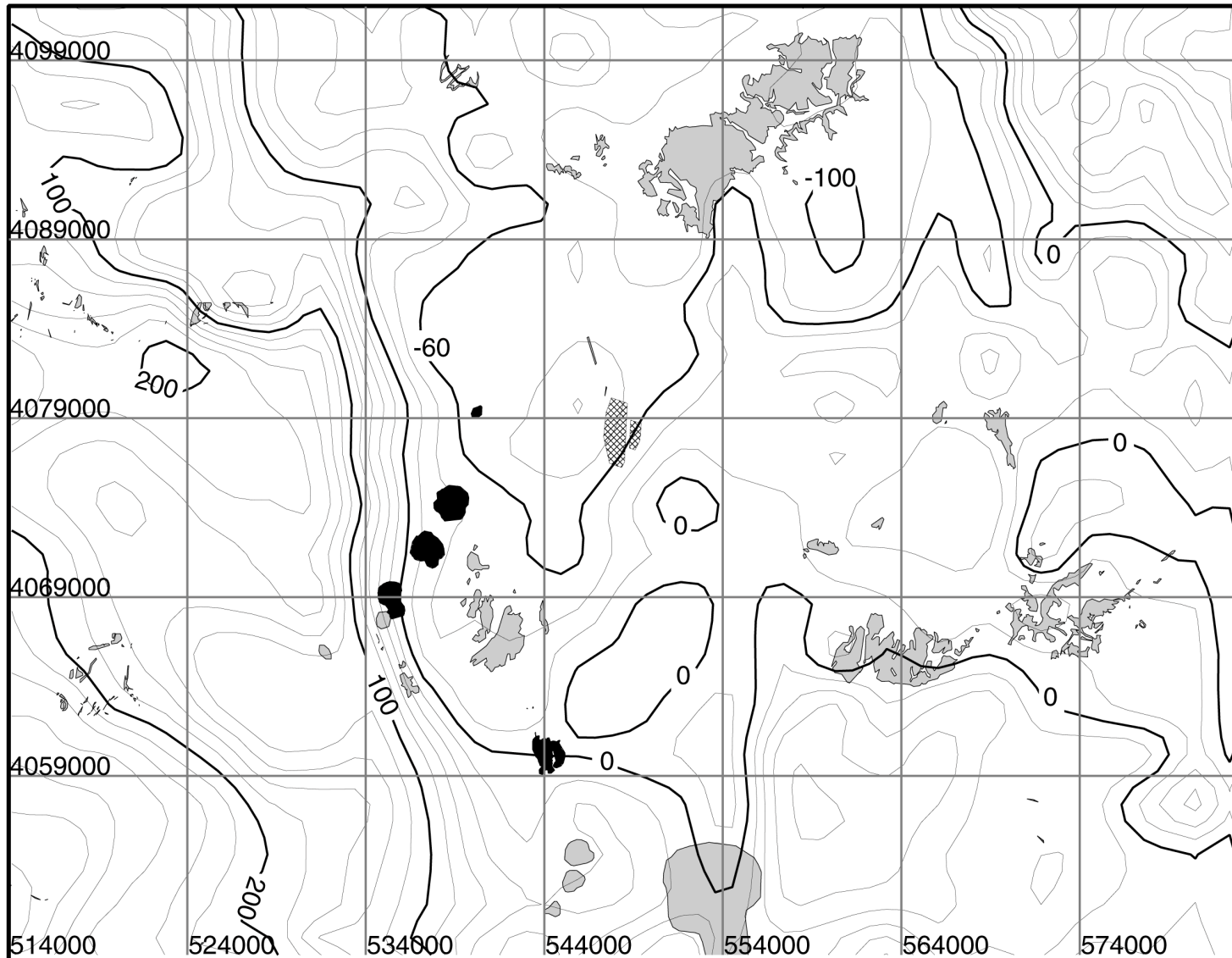


Figure 20. Apparent density variation across the Yucca Mountain region, derived from gravity data. Change from the mean apparent density in the map area is contoured in kg m^{-3} . Volcanoes tend to occur in areas of relatively low average density, east of the Bare Mountain fault.

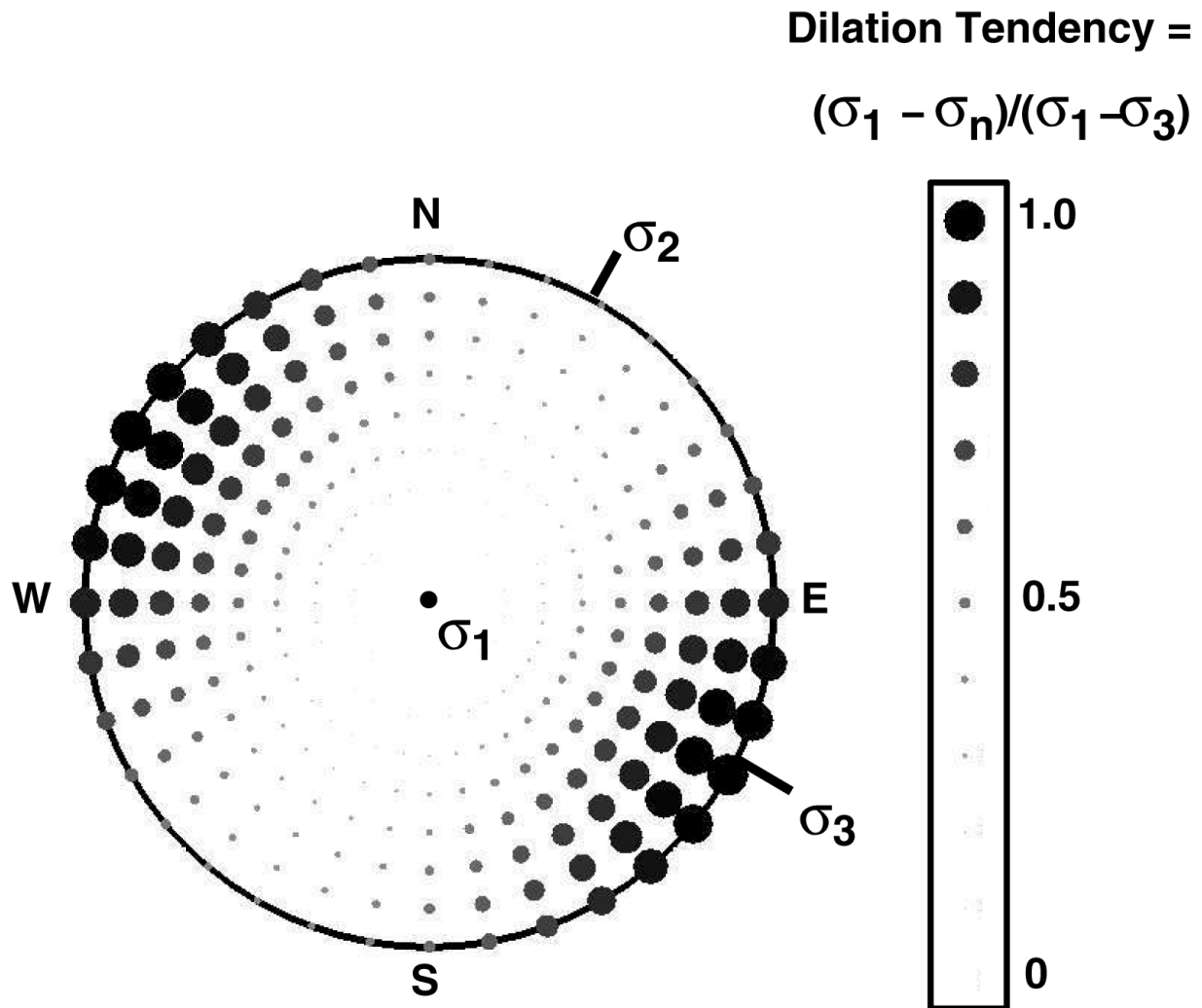


Figure 21. Schmidt plot of fault dilation tendency for Yucca Mountain region stresses. High dilation-tendency faults are oriented 355–085° with dips greater than 50° (cf. Figure 14).

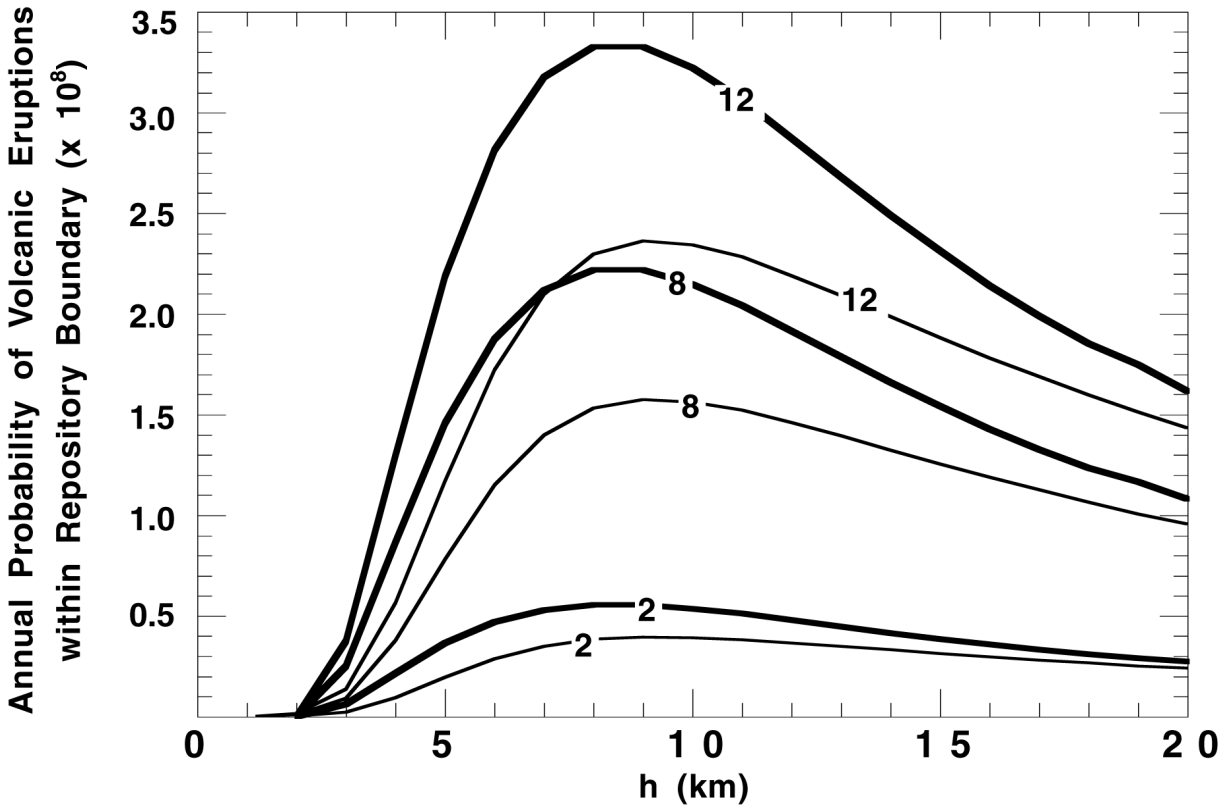


Figure 22. Annual probability of volcanic eruptions within the repository boundary. Igneous events are defined as individual mappable eruptive units and vents. A Gaussian kernel is used with smoothing parameter, h , varying from 0–20 km. Curves are shown for various regional recurrence rates of volcanic vent formation ($\lambda_t = 2 \times 10^{-6}$ v/yr, $\lambda_t = 8 \times 10^{-6}$ v/yr, $\lambda_t = 12 \times 10^{-6}$ v/yr), based on the distribution of Quaternary volcanoes (heavy lines) and Plio-Quaternary volcanoes (light lines). The effective repository area, A_e , is 5.49 km².

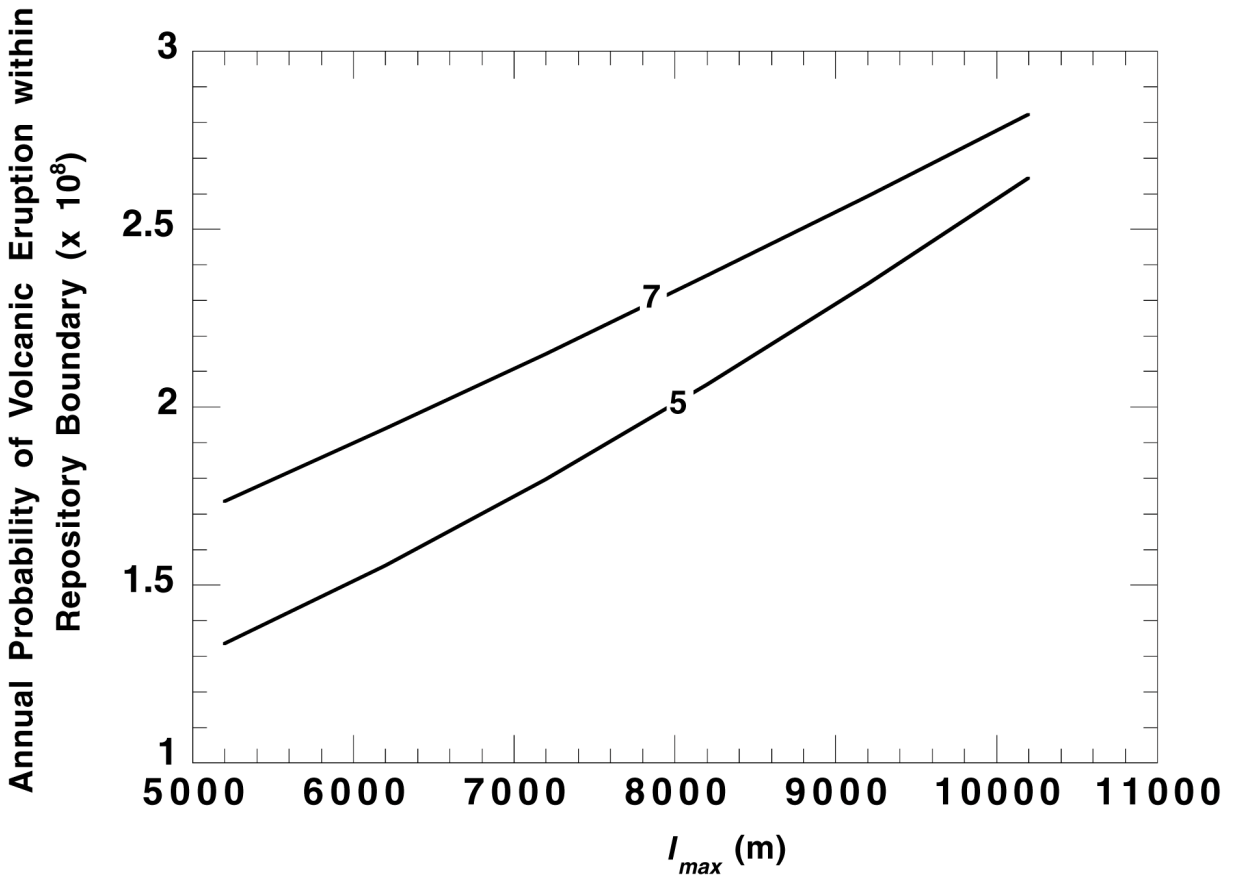


Figure 23. Annual probability of volcanic eruptions within the repository boundary. Igneous events are defined as vents and vent alignments. A Gaussian kernel is used with smoothing parameter, h , of 5 and 7 km (labeled lines) and is based on the distribution of three Quaternary igneous events. Vent alignment half-length, l_{max} , varied between 5200 and 10,200 m, roughly changing probability estimates by a factor of two. Probabilities are calculated using $\lambda_t = 3 \times 10^{-6}/\text{yr}$.

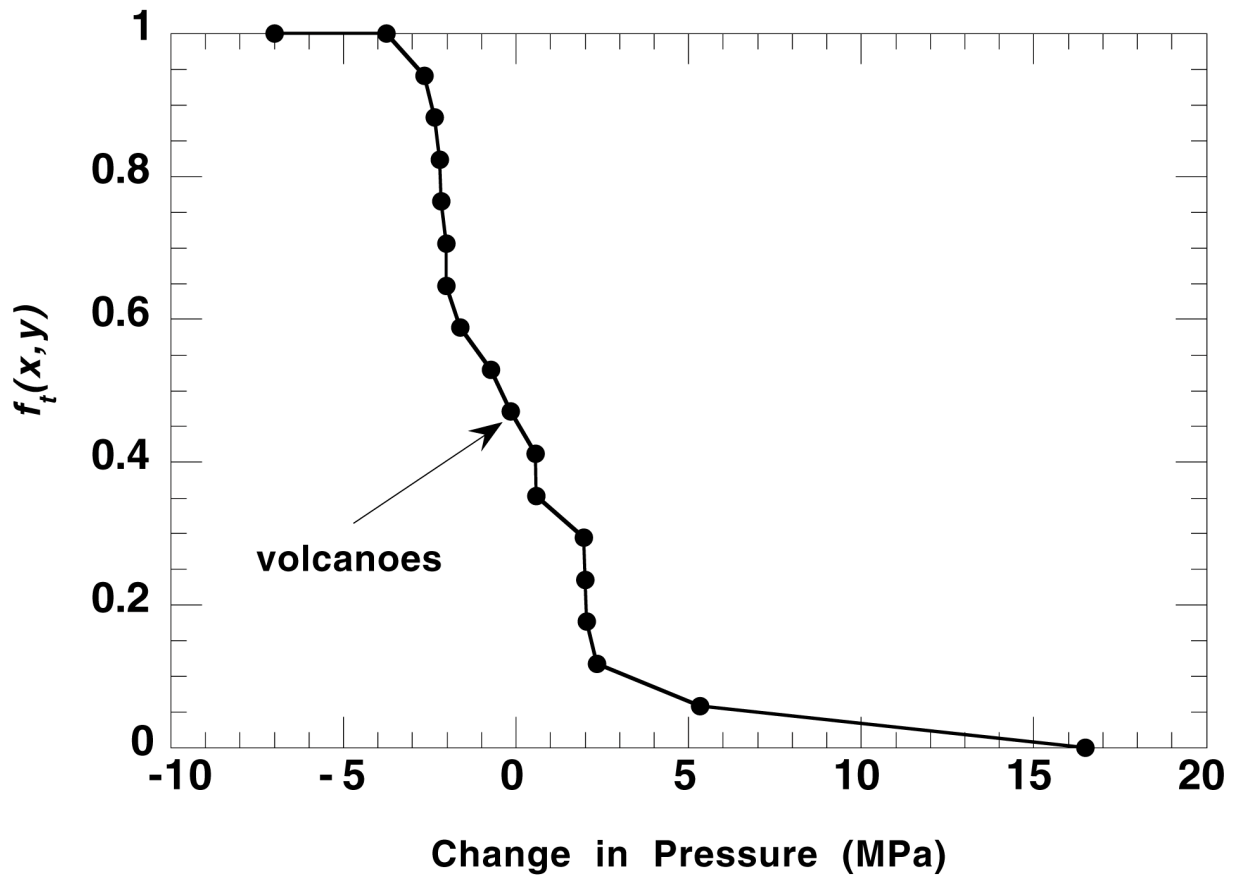


Figure 24. The weighting function, $f_t(x,y)$, is derived from changes in average crustal densities under the locations of Plio-Quaternary Yucca Mountain region volcanoes.

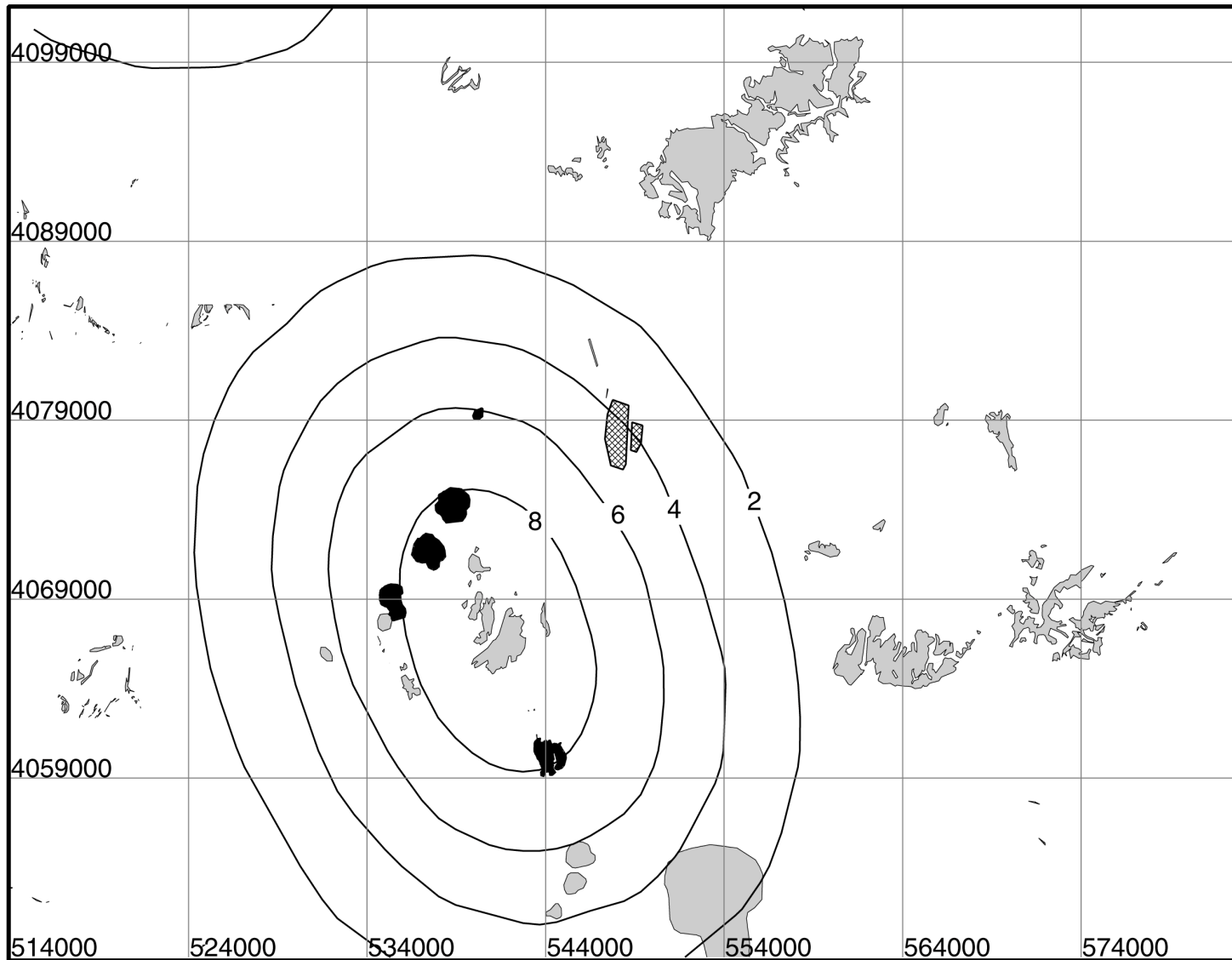


Figure 25. The spatial recurrence rate (v/km^2) is contoured in the area of Yucca Mountain using the Gaussian kernel function (Eq. 35). In this model, $h = 9000$ m and $N = 3$, based on the number of igneous events. The contour interval is $2 \times 10^{-4} v/\text{km}^2$. Other symbols are as in Figure 5.

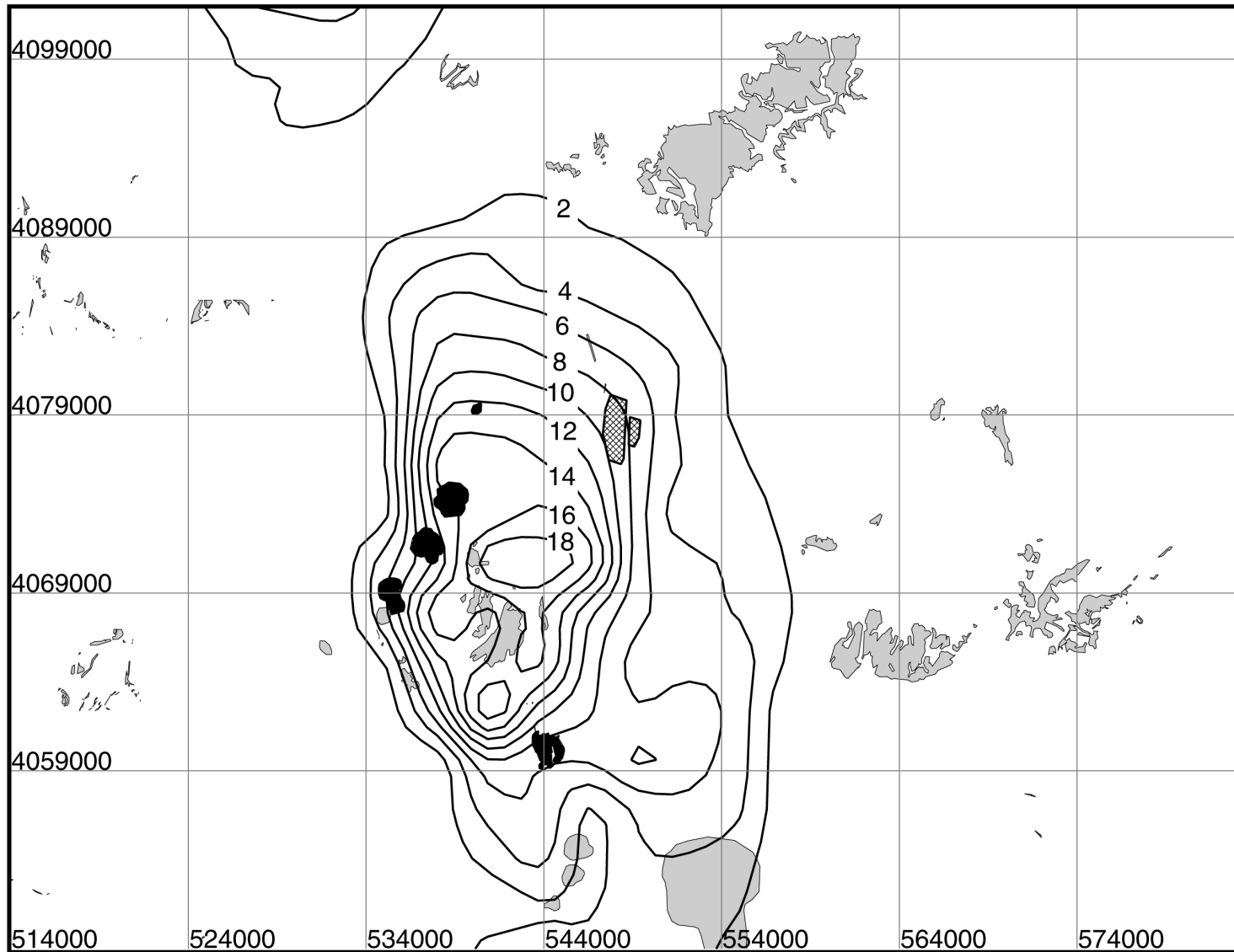


Figure 26. The spatial recurrence rate (v/km^2) is contoured in the area of Yucca Mountain using the modified Gaussian kernel function (Eqs. 37–39) to incorporate tectonic control on the probability estimate. In this model, $h = 9000$ m and $N = 3$, based on the number of igneous events. The contour interval is $2 \times 10^{-4} v/\text{km}^2$. Other symbols are as in Figure 5.

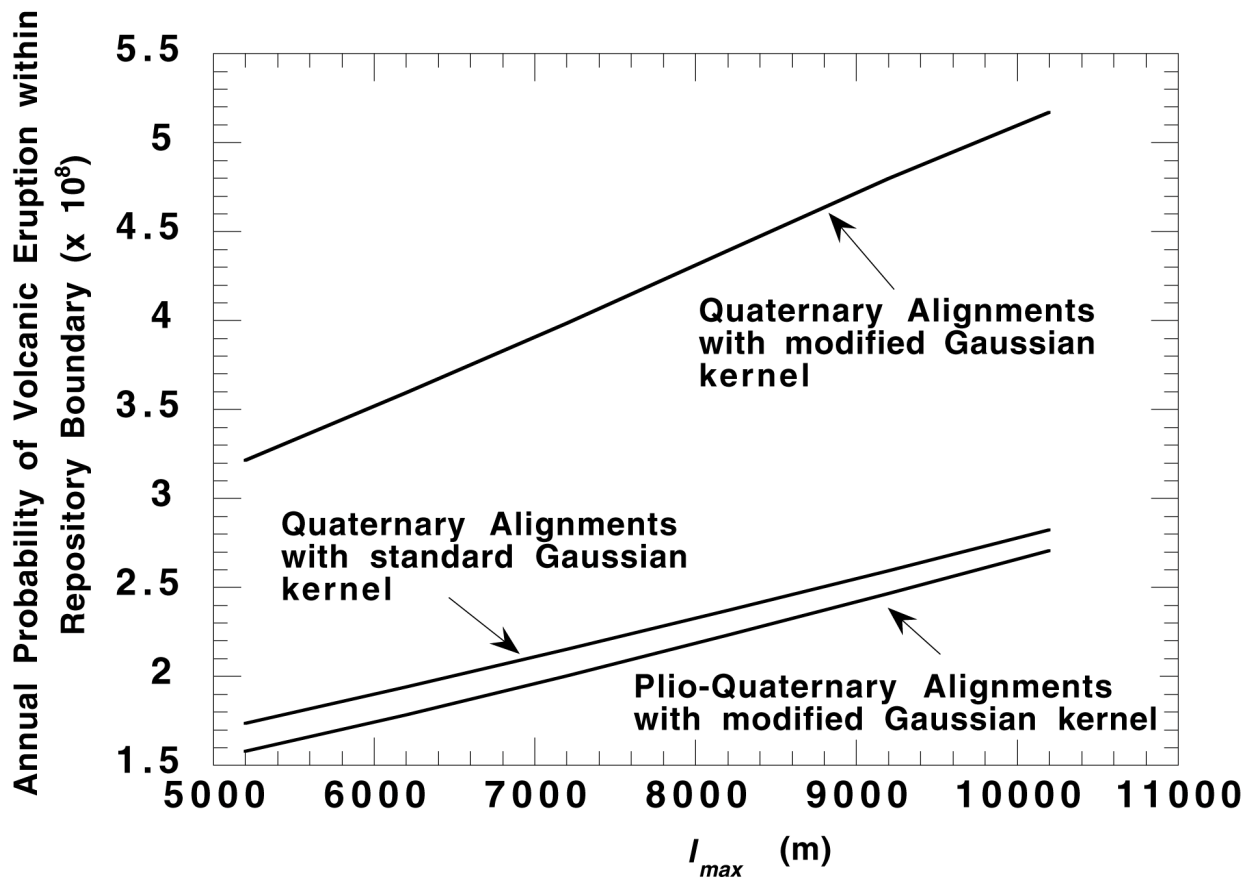


Figure 27. Annual probability of volcanic eruptions within the repository boundary using a modified Gaussian kernel. Igneous events are defined as vents and vent alignments. A modified Gaussian kernel is used with a smoothing parameter, $h = 7$ km, based on the distribution of three Quaternary igneous events. Vent alignment half-length, l_{max} , varied between 5200 and 10,200 m, roughly changing probability estimates by a factor of two. Probabilities are calculated using $\lambda_t = 3 \times 10^{-6}$ /yr. Curves are shown calculated using Plio-Quaternary events ($N = 12$) and the modified Gaussian kernel, and Quaternary events ($N = 3$) and the standard Gaussian kernel for comparison.

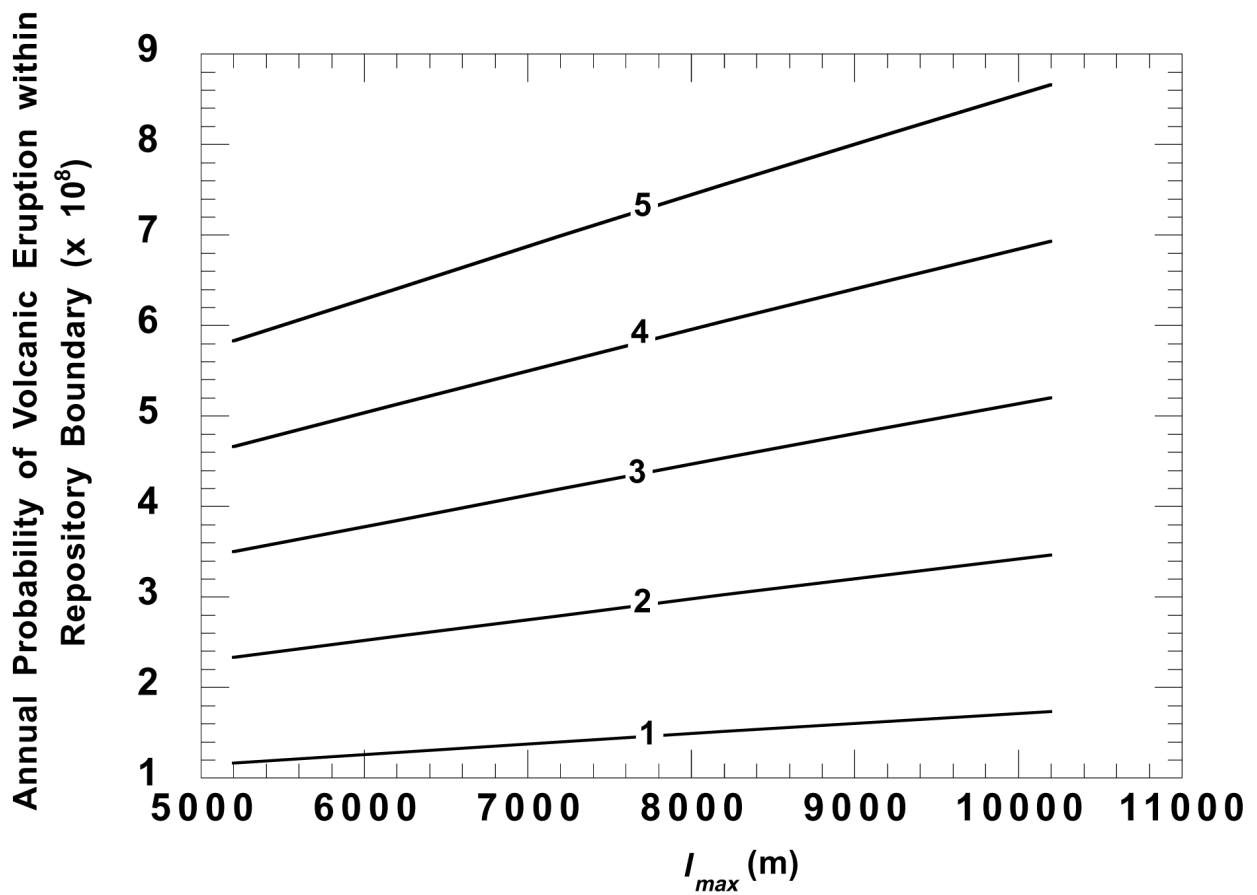
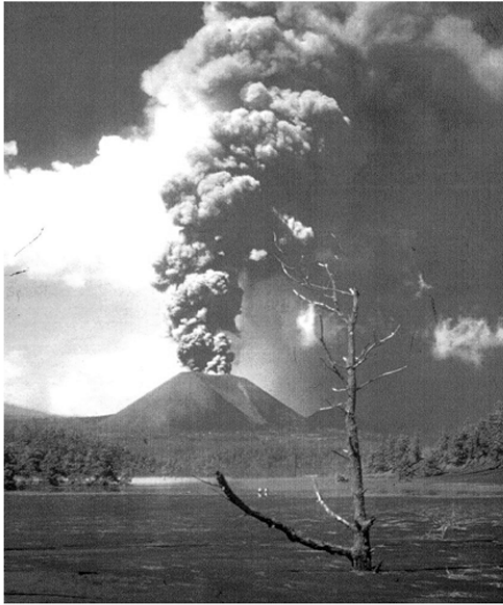


Figure 28. Annual probability of volcanic eruptions within the repository boundary using regional recurrence rates of $\lambda_t = 1 \times 10^{-6}$, 2×10^{-6} , 3×10^{-6} , 4×10^{-6} , and 5×10^{-6} /yr. Igneous events are defined as vents and vent alignments. A modified Gaussian kernel is used with smoothing parameter, $h = 7$ km, based on the distribution of three Quaternary igneous events.



1947 Parícutin, Mexico



1975 Tolbachik, Russia



1968 Cerro Negro



1995 Cerro Negro, Nicaragua

Figure 29. Tephra columns on erupting cinder cones. Columns vary from strong vertical columns with sustained gas-thrust regions and little deflection by the wind [e.g., 1947 Parícutin (McGregor and Abston, 1992), 1975 Tolbachik, and 1968 Cerro Negro] to weaker plumes with little or no gas-thrust region above the vent and that bend easily in the wind (e.g., 1995 Cerro Negro). Models that estimate the consequences of eruptions through the proposed repository need to quantify these varying styles of activity.

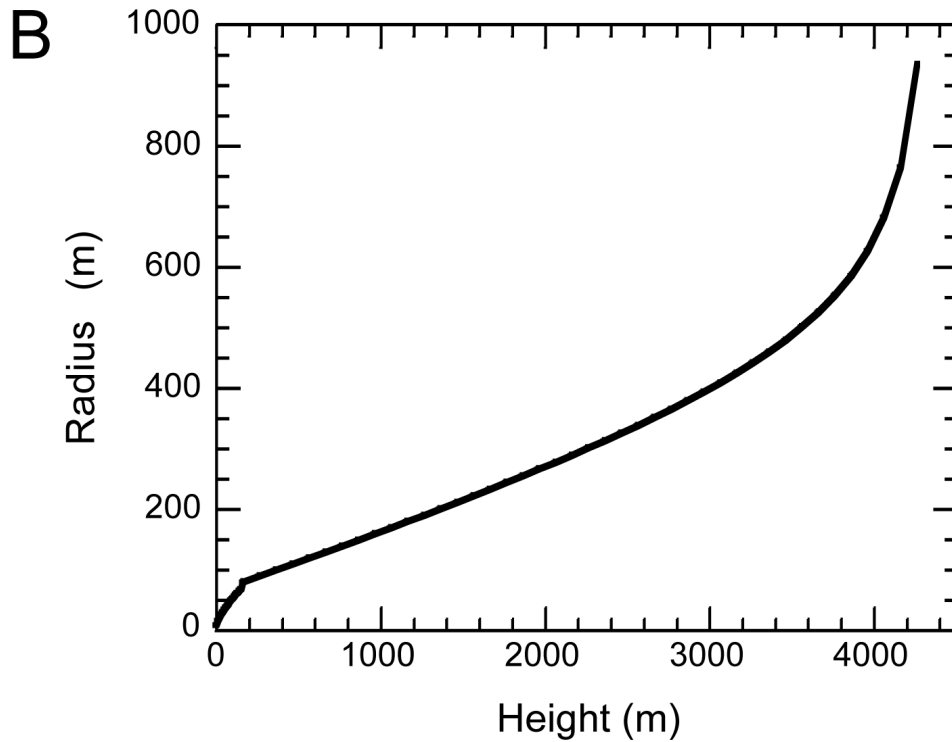
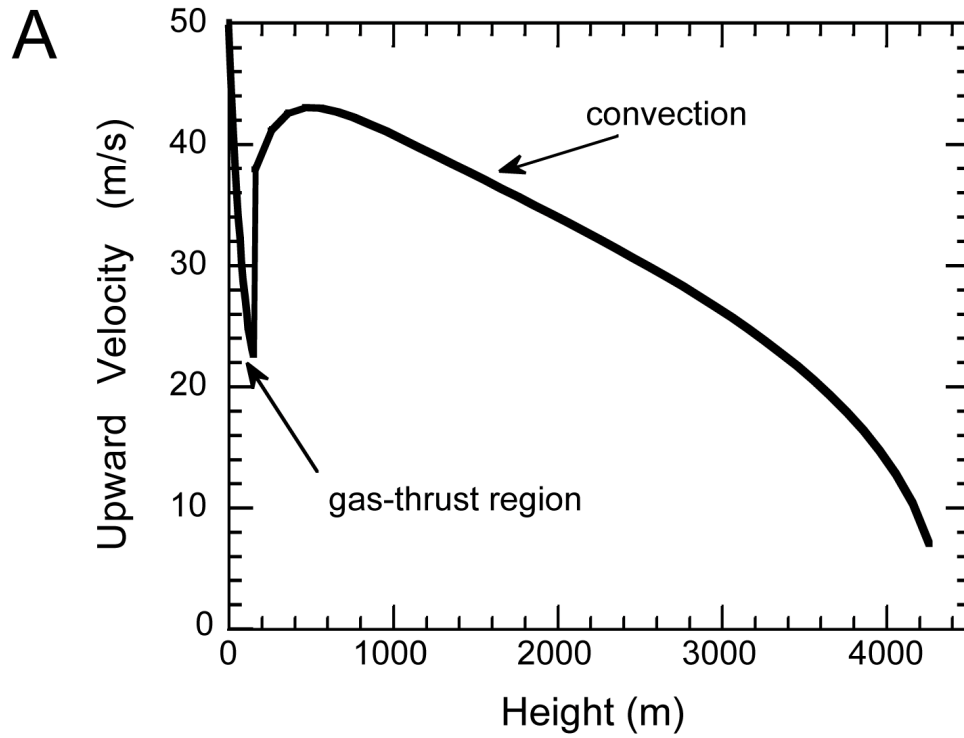


Figure 30. (a) Vertical velocity of particles in the volcanic column and (b) change in the column radius as a function of height for a violent strombolian eruption, based on the parameters in Table 1.

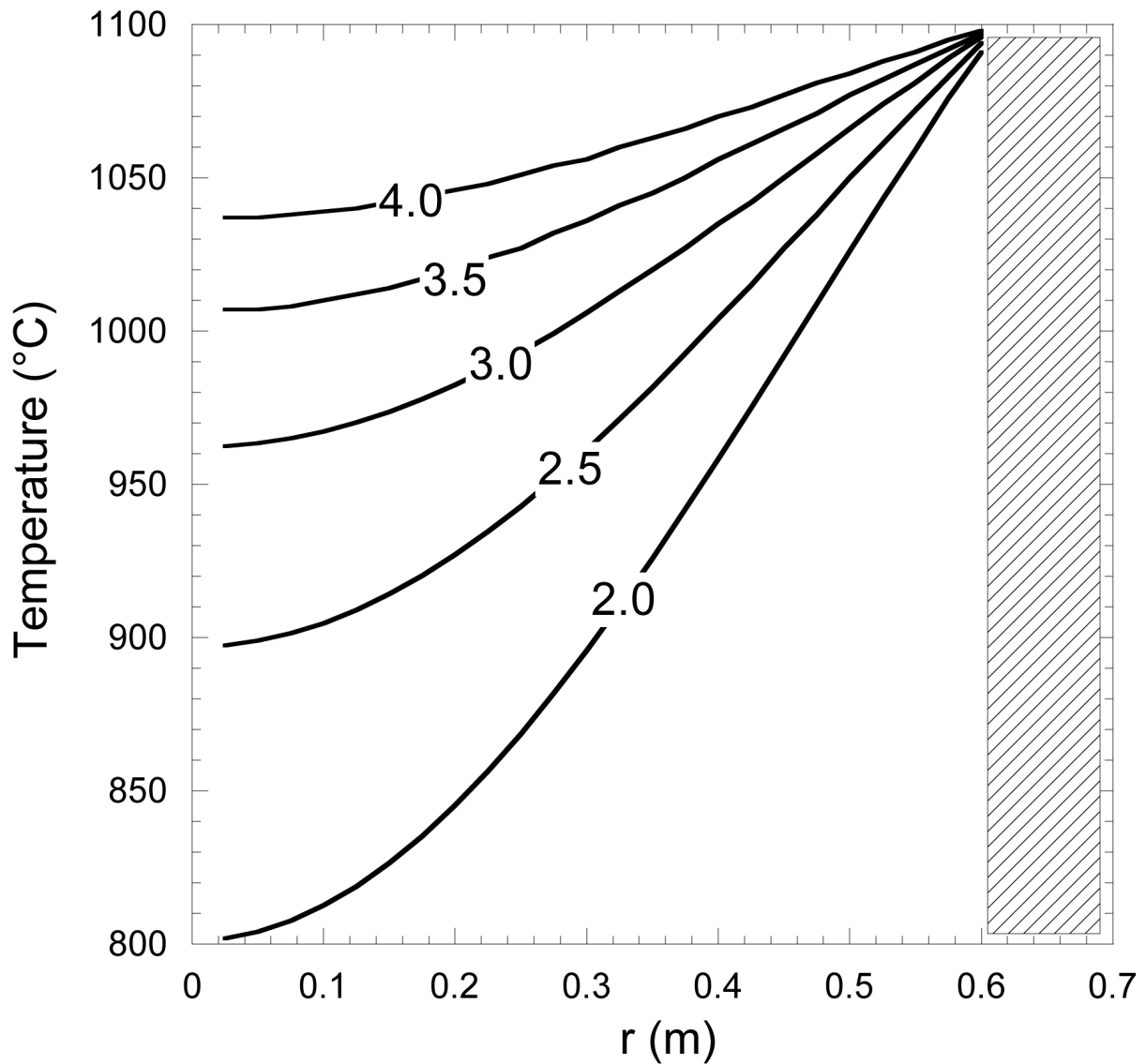


Figure 31. Temperature profiles inside the canister in near perfect thermal contact with a convecting magma at 1100 °C ($Bi = 50$; $T_i = 250$ °C, $T_f = 1100$ °C for a 1.2-m diameter canister). The canister is assumed to be infinite in length, which is a reasonable approximation for a cylinder five times longer than in diameter. Temperature profiles for times between 2 and 4 hr are shown. Centerline of canister at 0. Crosshatch area represents magma/canister boundary.

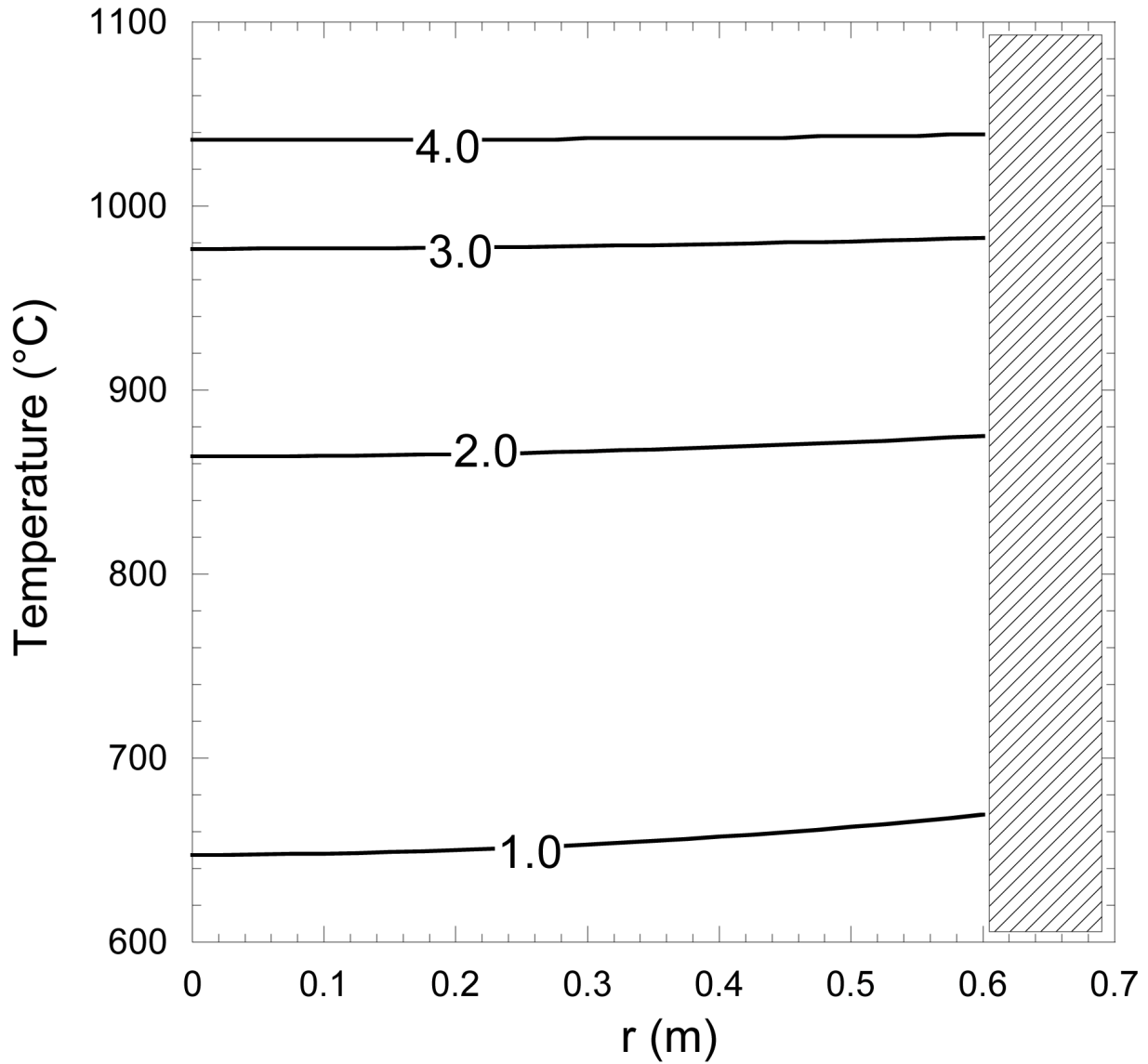


Figure 32. Temperature profiles inside the canister in poor thermal contact with a convecting magma at 1100 °C ($Bi = 0.1$; $T_i = 250$ °C, $T_f = 1100$ °C for a 1.2-m diameter canister). Temperature profiles for times between 1 and 4 days are shown. Centerline of canister at 0. Crosshatch area represents magma/canister boundary.

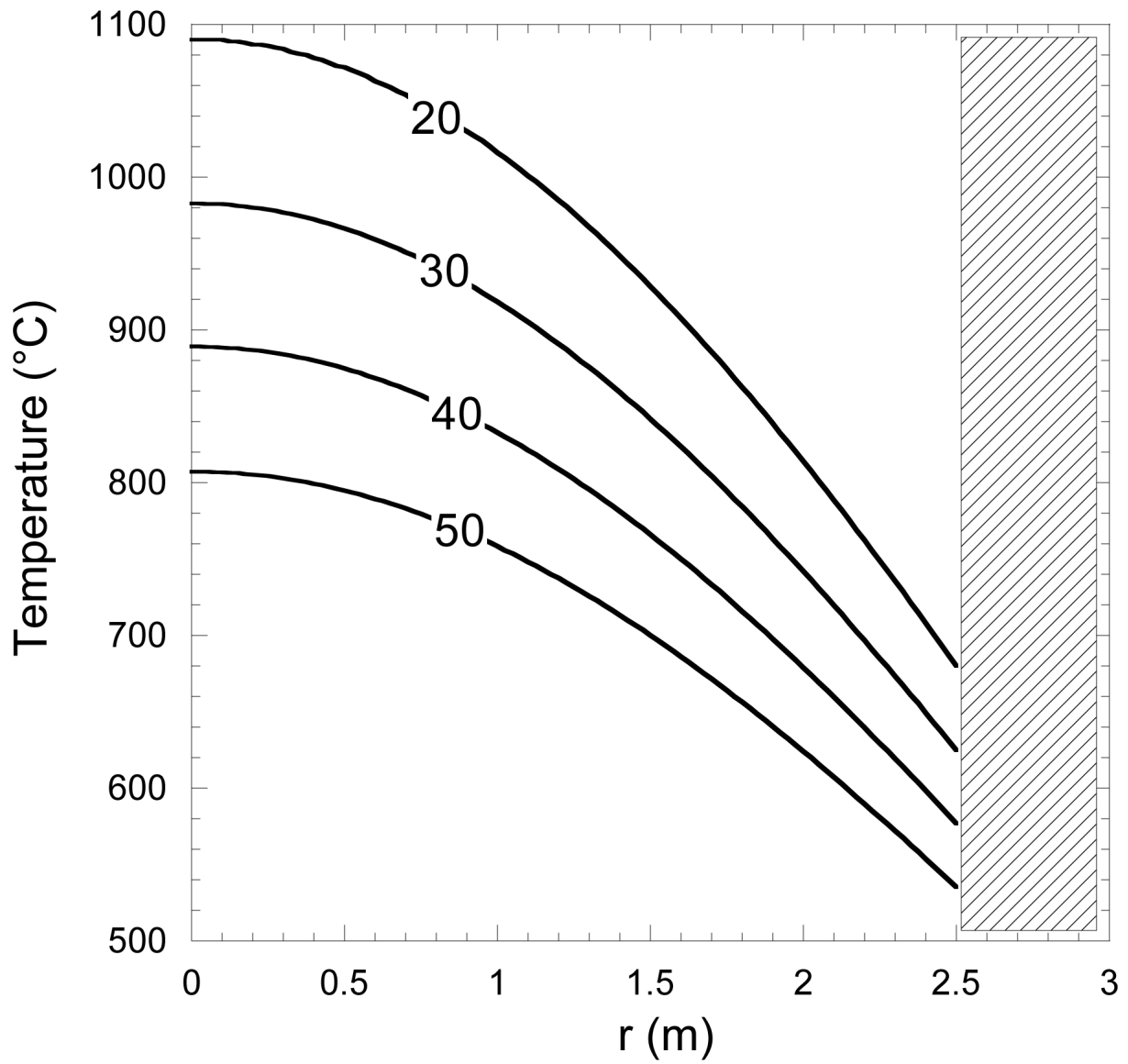


Figure 33. Temperature profile inside a magma-filled tunnel 20, 30, 40, and 50 days after magma emplacement. Centerline of the tunnel at 0. Crosshatch area represents tunnel wall.

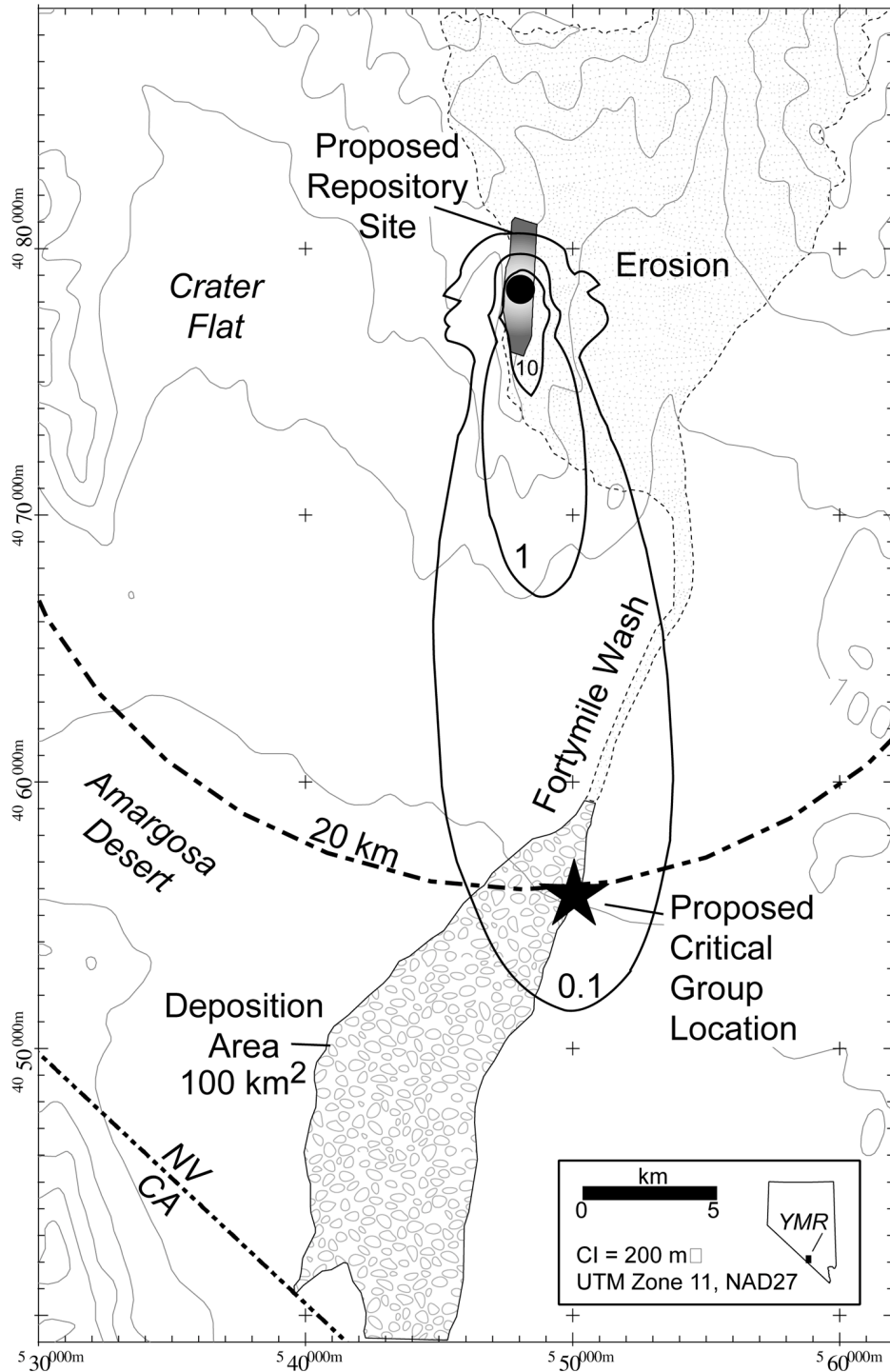


Figure 34. Scoping calculation for the remobilization of tephra following a small-volume volcanic eruption at the proposed repository site. Solid lines represent the depositional thickness of tephra from the eruption, in centimeters. 20-km boundary represents 20-m distance from repository outline shown in figure, with proposed critical group location following general guidance proposed in current regulations. Erosional and depositional outlines determined from U.S. Geological Survey 7.5' topographic maps.

